



Tectonics

RESEARCH ARTICLE

10.1029/2020TC006692

Key Points:

- River long-profile inversions show that northern Sicily experienced two time-transgressive base level falls since 4 Ma
- The base level fall pulses are related to the transit of the Calabrian forearc high during the opening of the Tyrrhenian Basin
- Relationships and feedbacks between tectonic forcing and geomorphic response are documented

Supporting Information:

Supporting Information may be found in the online version of this article.

Correspondence to:

F. Pavano, frp319@lehigh.edu

Citation:

Pavano, F., & Gallen, S. F. (2021). A geomorphic examination of the Calabrian forearc translation. *Tectonics*, 40, e2020TC006692. https://doi. org/10.1029/2020TC006692

Received 4 JAN 2021 Accepted 16 JUN 2021

A Geomorphic Examination of the Calabrian Forearc Translation

F. Pavano¹ and S. F. Gallen²

¹Department of Earth and Environmental Sciences, Lehigh University, Bethlehem, PA, USA, ²Department of Geosciences, Colorado State University, Fort Collins, CO, USA

Abstract The evolution of subduction forearcs as archived in the tectonic and geomorphic record serves to constrain geodynamic models of many convergent plate margins. This paper presents geomorphic stream channel metrics and river longitudinal profile modeling to assess geodynamic models describing the late Cenozoic horizontal translation of a Mediterranean forearc. The northern flank of Sicily is drained by roughly parallel north-flowing streams arranged across the hypothesized west-to-east migration path of the Calabrian forearc high. These streams present a snapshot of current geomorphic processes driven by spatiotemporal variations in crustal deformation, including river incision and landscape steepness. A stream power rule-based numerical modeling of the fluvial response time and knickpoint migration provides an independent prediction for the history of rock uplift associated with the translating forearc over the past ~4 Myr. The results serve as a test for two, crustal wave versus transformfault, end-member geodynamic models for the Calabrian forearc evolution, suggesting that our modeling supports the former. The river profile modeling shows that northern Sicily rivers experienced two pulses of time-transgressive rock uplift that progressively sweeps west to east. This analysis suggests the most rapid contemporary rock uplift rates are focused in NE-Sicily, where the forearc is currently located and where Pleistocene marine terraces indicate the highest rock uplift rates. These results are consistent with the west-to-east passage of a forearc high embedded in the subduction wedge, followed by a dynamic wave of rock uplift in its wake similar to what has been proposed for slab windows in other plate boundary settings.

1. Introduction

The tectonic setting of the Mediterranean basin features several convergent plate boundaries with small, highly arcuate subduction zones. Slabs in several of these subduction zones are rapidly rolling back (e.g., Doglioni, 1993), resulting in diverse kinematics of upper plate deformation, including paired compression and extensional fronts in overlying forearcs (Elter et al., 1975). The Calabrian Peninsula in southern Italy represents one such forearc where only the extensional domain is exposed above sea level today (D'Agostino et al., 2011; Tortorici et al., 1995). Calabria is widely thought to have rifted away from Sardinia 6 Ma, and rapidly translated eastward as the leading edge of a wave of the backarc extension that opened the Tyrrhenian Sea, following rollback of the Ionian subduction slab (Amodio Morelli et al., 1976; Rosenbaum & Lister, 2004; Figure 1). Several geodynamic and tectonic models, based largely on geophysical observations (e.g., Amodio Morelli et al., 1976; Bigi et al., 1991; Dewey et al., 1989; Finetti, 2005), have emerged to describe the rapid translation of Calabria and associated dynamic response of the asthenosphere to the subducted lithosphere. While some differences exist among these models, all predict a transient wave of crustal thickening and rock uplift in the forearc (Carminati & Doglioni, 2012; Faccenna et al., 2014), followed by extension in the back-arc region.

Existing, competing models for translation of Calabria make different predictions regarding the style and spatio-temporal history of crustal deformation recorded on the island of Sicily, which lies along the southern margin of Calabria's west to east migration track. Northern Sicily offers access to the structural and morphological record left behind in the passing wake of forearc migration, that is, otherwise submerged in the Tyrrhenian and Ionian seas. Despite numerous studies, it has proven difficult to link onshore structures to those recognized offshore that are associated with the forearc translation (Bianchi et al., 1987; Catalano et al., 2000, 2013; Finetti et al., 1996; Ghisetti & Vezzani, 1984; Lentini & Carbone, 2014; Lentini et al., 1994, 1996; Nigro et al., 2000; Renda et al., 2000).

© 2021. American Geophysical Union. All Rights Reserved.

PAVANO AND GALLEN 1 of 20

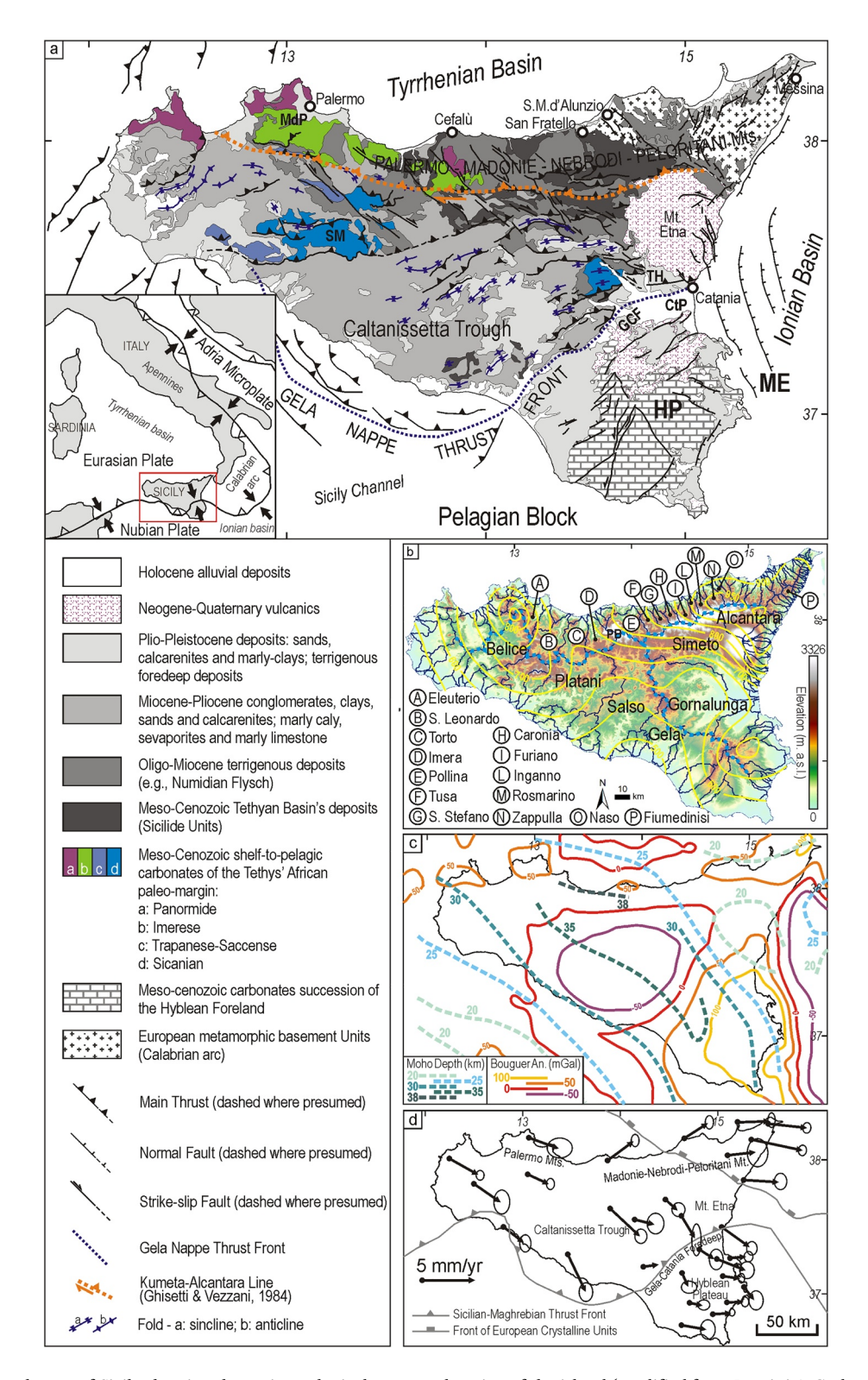


Figure 1. Geological sketch map of Sicily showing the main geological-structural setting of the island (modified from Lentini & Carbone, 2014 and after Pavano et al., 2015, 2019; Romagnoli et al., 2015). The inset frames the study area in the context of the Nubia-Eurasia Plates convergence. HP: Hyblean Plateau; SM: Sicanian Mountains; MdP: Palermo Mountains; GCF: Gela-Catania Foredeep; CtP: Catania Plain; TH: Terreforti High; ME: Malta Escarpment; (b) regional annual rainfall (mm/yr) gradient (yellow lines) averaged over 80 yr (1921–2003; Osservatorio delle Acque, 2005) overlapped to the elevation data. The main drainage basins are evidenced by blue lines. The main watersheds of the Island are labeled. PB: Piano Battaglia; (c) map showing the contouring of both the Moho depth (Dashed bold lines; modified from Giustiniani et al., 2018) and the Bouguer gravimetric anomaly (modified from Ferri et al., 2005); (d) Nubia referenced GPS velocity field of Sicily (modified from Mastrolembo Ventura et al., 2014).

PAVANO AND GALLEN 2 of 20



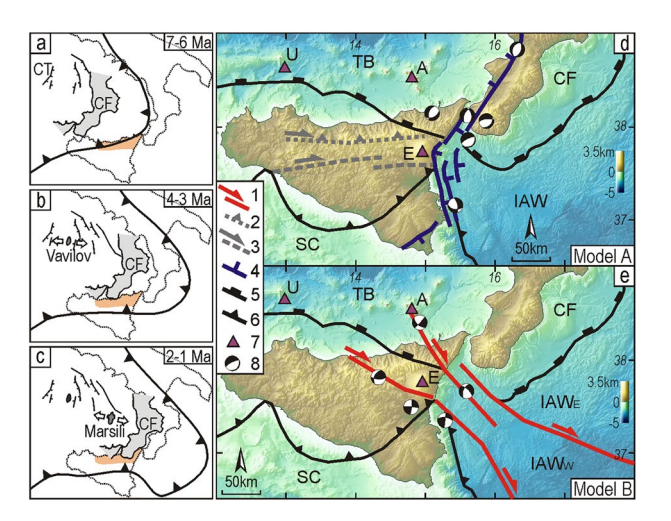


Figure 2. Sketch maps showing the primary end-members geodynamic models for the central Mediterranean area, emphasizing the migration of the Calabrian forearc. (a-c) Main stages of the Neogene-Quaternary evolution of the eastward migrating Calabrian forearc (CF) and the opening of the Tyrrhenian Basin showed together with the main volcanic centers development (Vavilov, Marsili; modified from Conti et al., 2017). The orange shaded area represents the PMNPM belt. The snapshots of the final stages are represented according to the two different end-members tested in the present study: (d) Model A and (e) Model B (see the text for more detail). Legend: 1: Right-lateral fault system of the STEP fault and Ionian accretionary wedge (Gutscher et al., 2019; Polonia et al., 2016); 2: Kumeta-Alcantara Line (Ghisetti & Vezzani, 1984); 3: Sicanian-Etna Line (Catalano, Pavano, et al., 2018); 4: Normal fault system of the riftlike extensional belt (Catalano et al., 2008; Monaco & Tortorici, 2000); 5: Front of the European crystalline units; 6: Front of the allochthonous Apenninic-Maghrebian units; 7: Volcanic centers (A: Aeolian Archipelago; E: Etna Volcano; U: Ustica); 8: Focal mechanisms (modified from Barreca et al., 2016; Loreto et al., 2012; Musumeci et al., 2005; Pondrelli et al., 2006; Scarfí et al., 2016). TB: Tyrrhenian Basin; SC: Sicilian Channel; CF: Calabrian Forearc; CT: Cornaglia terrace; IAW: Ionian Accretionary Wedge (E: eastern lobe; W: western lobe).

Late Cenozoic geodynamic evolution models used to explain the migration of the Calabrian forearc can be summarized by two end-members (Figures 2a-2e and 3a-3d). One end-member model (hereafter Model A) proposes that forearc migration proceeds through advection of crustal material through the subduction wedge (e.g., a crustal wave), accreting in the pro-wedge and stretching and fragmenting the forearc crust in the retro-wedge (Figures 3a and 3b; Catalano et al., 2008; Meschis et al., 2019; Monaco & Tortorici, 2000; Pavano et al., 2015). The southern lithospheric boundary of this crustal wave system would consist of W-E-oriented shear zones (e.g., Kumeta-Alcantara Line, Sicanian-Etna Line; Catalano, Pavano, et al., 2018; Ghisetti & Vezzani, 1984). The other end-member (hereafter Model B) proposed in several studies suggests that there are lithospheric-scale, NW-SE-oriented, right-lateral, transform faults embedded in the Sicilian mainland that are accommodating the migration of the Calabria forearc (Figures 3c and 3d; Barreca et al., 2016, 2019; Gallais et al., 2013; Gutscher et al., 2015; Polonia et al., 2011, 2016; Sgroi et al., 2012).

These two end-member models make specific and distinct predictions of the spatial and temporal patterns of deformation and rock uplift due to forearc migration. The crustal wave end-member scenario (Model A) predicts a smooth west-to-east migration of high uplift that progressively decays as the locus of deformation migrates with the rolling-back slab. In contrast, the transform-fault end-member scenario (Model B) suggests rock uplift progressively steps west-to-east as old transforms become inactive and new ones take over as the dominant structure accommodating forearc translation. Because landscapes transiently respond to changes in tectonic boundary conditions, the history of deformation, as expressed by changes in rock uplift rate, is encoded in the geomorphology of northern Sicily and specifically recorded in river profiles. A DEM-based geomorphic analysis of northern Sicily's river network evolution has been designed to identify rock uplift signals that can be used to test different models of the evolution of crustal structures and the geodynamics related to the hypothesized translation of the Calabrian forearc. A stream power rule-based numerical modeling of the fluvial response time and transient knickpoint migration provides independent estimates for time-transgres-

sive rock uplift over the past 4 Myr. Based on our river profile modeling results, we are able to discriminate between the competing geodynamic models. Within the context of these findings, we further analyze the topography to better characterize and constrain the geomorphic response to this time-transgressive tectonic forcing.

2. Tectonic and Geological Background

Sicily is situated in the Central Mediterranean at the boundary of African-European plate convergence (Dewey et al., 1989; Figure 1). The subduction-collisional complex of Sicily mostly consists of the SSE-vergent Sicilian fold-and-thrust belt (SFTB), an accretionary wedge composed of Tethyan and African-affinity crust that covers most of the island. To the south, these terranes were imbricated and thrusted during the Neogene over an African-affinity foreland carbonate platform (Pelagian Block; Burrollet et al., 1978) that outcrops in southeastern Sicily (Hyblean Plateau; Bianchi et al., 1987; Boccaletti et al., 1990; Roure et al., 1990; Figure 1a). This deformed sector (Bonforte et al., 2015) is separated from the subducting oceanic crust of the Ionian Basin by the Malta Escarpment (ME in Figure 1a), a Mesozoic lithospheric boundary. To the north, the internal sectors of the SFTB are overlain by European-affinity terranes (Lentini et al., 1995; Lentini & Vezzani, 1975).

PAVANO AND GALLEN 3 of 20



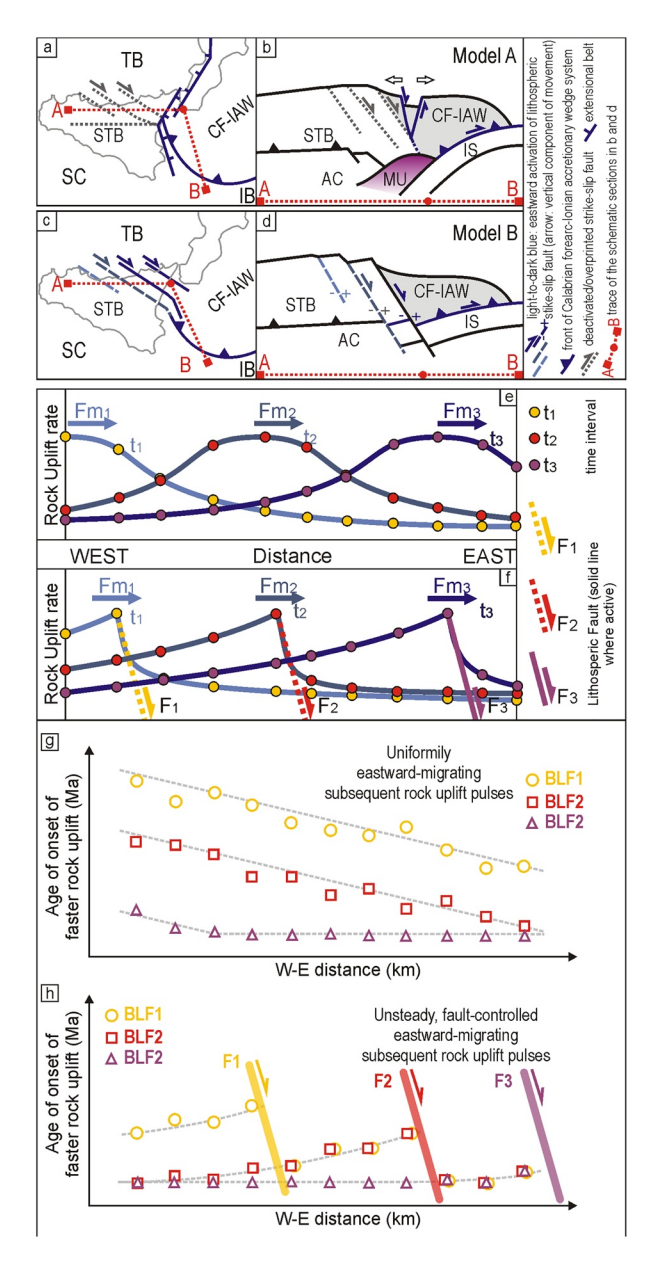


Figure 3. (a-d) Schematic cartoon simplifying, both in map view and cross-section, the two end-member models: Model A (a and b) and Model B (c-d). The two divergent white arrows in b indicate the extension in the area of the Messina Strait. TB: Tyrrhenian Basin; IB: Ionian Basin; SC: Sicily Channel; STB: Sicilian Thrust Belt; CF-IAW: Calabrian forearc-Ionian accretionary wedge; IS: Ionian Slab; AC: African Crust; MU: Mantle Upwelling due to the Ionian slab window. Below is a cartoon showing the spatial (west-to-east) and temporal (t1, t2, t3) distribution of the rock uplift rate predicted for the northern belt of Sicily by (e) Model A and (f) Model B. Fm_i: Forearc migration at stage i; (g and h) predicted west-to-east distribution of the onset of the rock uplift, both in the case of a uniform migration of tectonic pulse (g) and in the case of fault-controlled accommodation of nonuniform ("stepping" eastward) tectonic deformation (h). Every set of data (BLF1-3) shows the evolution of a single base level fall signal, both when uniformly migrating or when unsteadily controlled by faults. BLF: base level fall.

Emplacement of the accretionary wedge occurred during the Miocene opening of the Tyrrhenian Basin and east-southeastward migration of the Calabrian forearc (Amodio Morelli et al., 1976; Boccaletti et al., 1990; Dewey et al., 1989; Lentini et al., 1994; Malinverno & Ryan, 1986; Sartori et al., 2001). The Calabrian forearc moved obliquely across the carbonate platform (Faccenna et al., 2004), such that from west to east along the northern mountain belt of Sicily (PMNPM: Palermo-Madonie-Nebrodi-Peloritani Mts.), the deformed platform-to-wedge domains are juxtaposed (Figure 1a). Deformed carbonate platform and pelagic basin deposits of Africa affinity are widely exposed in the Palermo Mts. area in the west (Catalano & D'Argenio, 1982; Lentini et al., 1994), Meso-Cenozoic accretionary wedge chaotic terrains (e.g., Sicilide Unit) and Paleogene terrigenous deposits (e.g., Numidian Flysch) are exposed in the Madonie-Nebrodi Mts. in the middle (Lentini et al., 1994; Roure et al., 1990), and the Europe-affinity Hercynian crystalline basement terranes are exposed to the east in the Peloritani Mts (Ben Avraham et al., 1990; Catalano, Cirrincione, et al., 2018; Lentini et al., 1994, 2000; Figure 1a). To the south of the PMNPM, progressive emplacement of the accretionary wedge includes several Miocene-to-Pleistocene wedge-top basin sedimentary sequences (Decima & Wezel, 1971; Di Grande & Giandinoto, 2002).

Geophysical (Bianchi et al., 1987; R. Catalano et al., 2013; Chironi et al., 2000; Ferri et al., 2005; Giustiniani et al., 2018) and geodetic data (e.g., Mastrolembo Ventura et al., 2014; Figures 1c and 1d) show that the main lithospheric structural architecture of the SFTB is characterized by E-W- to ENE-WSW-oriented, regional, oblique dextral thrust ramps (Catalano, Pavano, et al., 2018; Ghisetti & Vezzani, 1984). In northern Sicily, the PMNPM crudely corresponds to the axial zone of the thrust-ramp anticlines related to the Kumeta-Alcantara Line (Ghisetti & Vezzani, 1984; Gueguen et al., 2002; Renda et al., 2000; Figure 1a).

Since the late Miocene, NW–SE-trending right-lateral shear zones progressively propagated eastward, following the translation of Calabria (Finetti et al., 1996; Lentini et al., 1995, 2000), and accommodated the Plio-Pleistocene opening of the Tyrrhenian Basin (i.e., Vavilov and Marsili stages; Kastens et al., 1988; Malinverno, 2012; Rosenbaum & Lister, 2004; Figures 2a–2c). After the early development of the Cornaglia Terrace (CT) to the east of Sardinia and the deposition of the Messinian salts (Malinverno et al., 1981; Figure 2a), the E-W-trending rifting processes shifted eastward (7–5 Ma; Figure 2a), and the spreading center of the Vavilov basin developed (4–3 Ma; Conti et al., 2017; Kastens et al., 1988; Figure 2b). Starting from 2 Ma, the NW–SE-oriented spreading (Sartori, 2003) further shifted toward the southeast to the younger Marsili Basin (Kastens et al., 1988; Figure 2c), influencing the dynamics of the peri-Tyrrhenian belt also during the late Pleistocene (Antonioli et al., 2006; Catalano & Di Stefano, 1997; Ferranti et al., 2010).

2.1. Competing Tectonic Models and Their Geomorphic Predictions

In the framework of the general Neogene-Quaternary geodynamic evolution of the study region described above, two end-member tectonic models (Model A and Model B) have emerged to explain late Pleistocene-Holocene faulting and active seismicity in Sicily (Figures 2d and 2e). Model A suggests that the Calabrian forearc migrated as a crustal wave to its current

PAVANO AND GALLEN 4 of 20



position in eastern Sicily. The early stage of the forearc migration was supposedly accommodated along its southern edge by W–E-trending shear zones (Figure 2d; e.g., Kumeta-Alcantara Line, Sicanian-Etna Line; Catalano, Pavano, et al., 2018; Ghisetti & Vezzani, 1984). Starting in the late Pleistocene, the forearc was fragmented by a NNE- to NNW-striking extensional belt (Catalano et al., 2008; Monaco & Tortorici, 2000; Figures 2d, 3a, and 3b), thought to be related to mantle upwelling processes at depth (e.g., Catalano et al., 2010; Figure 3b), that accommodates ongoing eastward translation of the forearc.

In contrast, Model B predicts dominant NW–SE-trending strike-slip (dextral) fault systems (Figures 2e, 3c, and 3d). Since the Pliocene, these shear zones cut across major topographic and geologic boundaries on-shore from the Tyrrhenian to the Ionian side of the Island, especially across NE-Sicily (Argnani & Bonazzi, 2005; Barreca et al., 2016, 2019; Gallais et al., 2013; Gutscher et al., 2015; Polonia et al., 2011, 2016; Sgroi et al., 2012; Figures 2e, 3c, and 3d). These hypothesized structures are argued to continue in the Ionian offshore, where they have been imaged in the bathymetry and accretionary wedge sediments (e.g., Argnani & Bonazzi, 2005; Barreca et al., 2019; Nicolich et al., 2000; Polonia et al., 2016).

Each of these end-member tectonic models predicts distinct spatio-temporal rock uplift histories along northern Sicily (Figures 3e and 3f). Importantly, these different uplift histories elicit diagnostic landscape responses that can be measured and tested through analysis of river profile geometries (e.g., channel steepness index, and knickpoints). The W–E distribution of a series of N–S-oriented drainage systems is ideally situated to record the spatial and temporal history of tectonically driven rock uplift capable of distinguishing between these end-members. The fluvial networks will record this history as geomorphic transience, including variations in steepness, drainage divide mobility, and modeled age of base level fall-related knickpoints, which we evaluate in this study.

Model A (Figures 2d, 3a, and 3b) predicts the transit of a wave of rock uplift; thus, the theoretical age of the onset of a base level fall (measured by the river response time; see the Section 3 for details) is predicted to young progressively toward the east. Assuming that more than one base level fall event is triggered in this scenario, we expect similar west-to-east time transgressive patterns of knickpoint migration paced by the rate of forearc migration. When plotted in time since base level fall versus distance along the coast, multiple events will plot as parallel sloping lines, where the slope of each line equals the rate of forearc migration (Figure 3g). Conversely, Model B (Figures 2e, 3c, and 3d) predicts non-uniform, repeatedly interrupted patterns in rock uplift from west to east (Figures 3f and 3h) associated with the location of hypothesized NW–SE-trending strike-slip faults cross-cutting the entire PMNPM belt and progressively activating eastward (Figures 3c, 3d, 3f, and 3h).

3. Methods

ArcGIS 10.6 was used to analyze a 20-m resolution digital elevation model (DEM) provided by ISPRA (2004; www.sinanet.isprambiente.it). An upslope area of 1 km² was set as the channel-head threshold in defining the drainage network (Montgomery & Foufoula-Georgiou, 1993; Wobus et al., 2006). Channels were extracted from the drainage network and modeled using the Matlab-based TopoToolbox and TAK software packages (Forte & Whipple, 2019; Schwanghart & Scherler, 2014, 2017).

3.1. Drainage System Analysis: $k_{\rm sn}$, X-Map and River Profile Response Time (τ)

Empirical observations from river channels thought to be graded or near equilibrium demonstrate a power law relationship between channel slope (S) and drainage Area (A; m^2), a proxy of drainage discharge (Flint, 1974; Hack, 1957; Kirby & Whipple, 2001; Snyder et al., 2000),

$$S = k_{\rm s} A^{-\theta} \tag{1}$$

where k_s is the channel steepness index and θ is the concavity index. This relationship, commonly referred to as Flint's law, provides a framework for interpreting tectonics from topography based on the stream power incision rule (Howard & Kerby, 1983). The stream power rule describes long-term bedrock channel erosion (E) as power functions of drainage area and local channel slope scaled by a constant of erodibility (K):

PAVANO AND GALLEN 5 of 20

$$E = KA^m S^n. (2)$$

where m and n are positive constants that reflect incision process, hydrology, and channel hydraulics (e.g., Whipple et al., 2000; Whipple & Tucker, 1999). Equation 2 can be solved for local channel slope and rearranged into a similar form as Equation 1 where:

$$S = \left(\frac{E}{K}\right)^{1/n} A^{-m/n}.\tag{3}$$

Comparison of Equations 1 and 3 shows that the steepness index k_s ($m^{2\theta}$) is a function of erosion rate, or at steady state rock uplift rate (U; mm/yr), and rock erodibility (K; m^{1-2m} yr⁻¹; Kirby & Whipple, 2001; Snyder et al., 2000; Wobus et al., 2006). θ is related to the ratio of m and n, which under steady-state conditions, assumes a theoretical value of 0.45 (Whipple, 2004; Whipple & Tucker, 1999). Assuming that rock uplift (U) equals channel erosion (E) and E0 and E1, which is consistent with plucking-dominated, detachment limited channel erosion processes (Hancock et al., 1998), a simple relationship between channel steepness (E1, E2, E3, E3, E4, and E4 emerges:

$$k_s = (U / K). \tag{4}$$

This relationship is useful because k_s is readily determined from analysis of digital topography, and, if the above assumptions are reasonably correct, one can interpret k_s in terms of changes in rock uplift rate or erodibility. Equation 4 is used here to calibrate the basin per basin distribution of coefficients of rock erodibility along the northern belt of Sicily. We used the k_s averaged at a basin-scale and assume that the long-term rock uplift rate, varying west to east along north Sicily (e.g., Arisco et al., 2006), is consistent with the marine terraces-derived long-term uplift rate, and uniform for each catchment, as well as equal to the catchment's long-term rate of erosion. Despite the timing and the location of the knickpoints along the drainage network, the averaging of k_s responds to the occurrence of all the transients distributed along the channels, an approach reliable for the scope of the paper. We use the estimated K as constant throughout each drainage basin following the unification of almost similar rock types or comparable lithological units.

A complementary approach to model stream long profiles (Perron & Royden, 2013) accounts for the integration of a rearranged version of Equation 1 with respect to distance (x):

$$z(x) = z(x_b) + k_s A_0^{-m/n} \chi, \tag{5a}$$

where

$$\chi = \int_{x_b}^{x} \left(\frac{A_0}{A(x')} \right)^{m/n} dx', \tag{5b}$$

and z(x) and $z(x_b)$ are the elevations at distance x and at base level (x_b) , respectively, and A_0 is an arbitrary scaling area. The integral term, χ (Chi), is a transformed coordinate along the river network with units of length (Perron & Royden, 2013). The m to n ratio is equivalent to the concavity index, θ , in Equation 1. Assuming uniform U and K (Giachetta & Willett, 2018), Equation 5a is related to Equation 2 and, being integrated, provides a prediction of the steady-state channel elevation z(x) (Gallen & Thigpen, 2018). Note that Equation 5a is that of a line where the slope of plots of χ versus elevation, or χ -plots, is proportional to the steepness index, k_s (Perron & Royden, 2013).

Because k_s and θ covary and because θ is thought to be insensitive to uniform vertical tectonic forcing, the steepness index (k_s) is commonly normalized (k_{sn}) according to a reference concavity (θ_{ref}) , usually corresponding to the average value of 0.45 based on empirical studies and theoretical considerations (Wobus et al., 2006). In the present study, a normalized channel steepness map was generated using a reference concavity of 0.45 (Snyder et al., 2000; Wobus et al., 2006) with Topotoolbox-2 (Schwanghart & Scherler, 2014, 2017). The k_{sn} map was then interpolated by kriging in ArcGIS to maximize its lateral continuity, and it was spatially compared with mapped geology (e.g., Lentini & Carbone, 2014), Plio-Pleistocene rock

PAVANO AND GALLEN 6 of 20



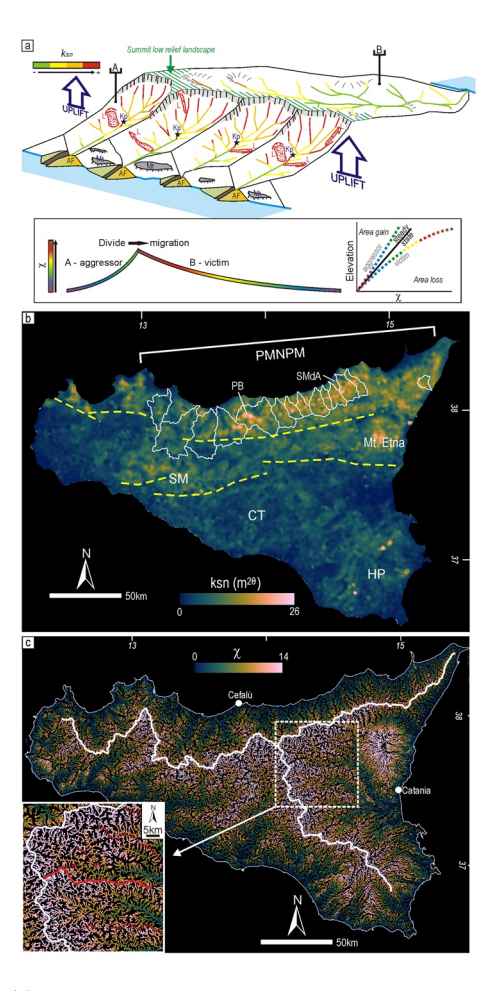


Figure 4. (a) Cartoon showing how the main geomorphic metrics (e.g., $k_{\rm sn}$, χ) and features distribute across a mountain range preserving summit low-relief landscape and how the drainage system numerically responds to cross-divide differential morphodynamics. The schematic drainage network in the main frame shows a color ramp according to the ideal changes in $k_{\rm sn}$. The plot at the bottom shows the ideal alongstream distribution of χ at the two sides of the mountain ridge. In the inset is the relationship between the aggressor and victim drainage basins, in a non-steady state (divide roaming) conditions. AF: Alluvial Fan; Mt: Marine terrace; Kp: Knickpoint; L: Landslide; (b) distribution pattern of the normalized channel steepness index (k_{sn}) interpolated by kriging technique. The drainage basins of the northern side of Sicily are also shown (outlined in white). The dashed lines represent the main geomorphic boundaries. PMNPM: Palermo-Madonie-Nebrodi-Peloritani Mts.; SM: Sicanian Mts.; HP: Hyblean Plateau; CT: Caltanissetta Trough; PB: Piano Battaglia; SMdA: San Marco d'Alunzio; (c) Spatial distribution of χ-map. The main drainage divides of the Island are also reported (drawn in white). The inset shows a χ-map detail for the central eastern Sicily, framed by the dashed box in the main map. The red lines indicate southward roaming divides (solid: main basin divides; dotted: tributaries divides).

uplift rates obtained from the elevation of marine sediments above sea level (Arisco et al., 2006; Catalano & Di Stefano, 1997; Ferranti et al., 2010), and regional rainfall distributions (Osservatorio delle Acque, 2005).

Under uniform rock type and climate conditions, variations in $k_{\rm sn}$ can be interpreted to reflect the channel response to base level fall (rock uplift) as transient knickpoints. Under these conditions, χ predicts how the transient signal of the base level fall impact the dynamics of drainage divides, which are predicted to move in the direction of the higher χ values for opposing channel heads (Forte & Whipple, 2018; Whipple et al., 2017; Willett et al., 2014; Figure 4a). The χ analysis for Sicily, as applied elsewhere (e.g., Willet et al., 2014), can be used to test the drainage network's response to tectonic deformation.

Under conditions of uniform erodibility and when $n=1,\chi$ is a proxy for the fluvial response time (τ ; Whipple & Tucker, 1999), which is the time it takes for a signal (e.g., base level fall or change in erosivity) to propagate upstream based on the kinematic wave equation represented by the stream power model (Rosenbloom & Anderson, 1994; Whipple & Tucker, 1999). With these assumptions, when calibrated using estimations of bedrock erodibility (K), χ can be transformed into τ (Equation 6) and utilized along with channel elevation data to provide base level fall histories (Fox et al., 2014; Gallen, 2018; Goren et al., 2014; Pritchard et al., 2009; Roberts & White, 2010). In this case, the τ position of a knickpoint along a river network represents the time since the perturbation (e.g., a change in tectonic rock uplift rate) affected the outlet of the drainage basin.

We perform the linear river profile inversions based on the "block uplift" method of Goren et al. (2014; described below) using Matlab code (Gallen, 2018) that leverages TopoToolbox-derived stream networks available in the Zenodo repository publisher (see Acknowledgements section for references). Assuming spatially uniform but temporally varying rock uplift rates (e.g., block uplift), the history of base level fall will be manifest as upstream migrating patches of variable steepness in plots of τ versus elevation (Goren et al., 2014; Pritchard et al., 2009; Roberts & White, 2010). Importantly, when n = 1, this block uplift model can be discretized by increments of χ or τ and organized into a linear system of equations in χ -z or τ -z space that can be inverted for the relative or calibrated history of rock uplift, respectively (see Goren et al., 2014 for a complete discussion). We want to emphasize that this inversion is effectively using linear inverse theory to calculate the average $k_{\rm sn}$ in discretized bins of χ ; assumptions related to n = 1 and spatially and temporally uniform erodibility allow interpretation of these changes in terms of uplift rate (see Equation 4) and time when properly calibrated. With this in mind, spikes in plots of U versus χ or τ represent locations of elevated steepness in the -transformed river network that are interpreted as genetically related knickpoints propagating upstream through the river system.

Following Goren et al. (2014), we assume that n = 1 in the studied basins and inverted χ -transformed river long profiles to derive relative rock uplift histories for each of the basins draining the northern coast of Sicily.

 χ and the relative rock uplift history (U^*) were converted to scaled units of fluvial response time and rock uplift rate using an erodibility term calculated independently for each drainage basin. The erodibility term (K) was calculated using Equation 4 and the average drainage basin steepness (defined as the basin average $k_{\rm sn}$) and the average long-term rock uplift rate from uplifted marine sediments for each basin draining the northern Sicilian coastline (Figure S3 and Table S3).

PAVANO AND GALLEN 7 of 20

10.1029/2020TC006692

The fluvial response time is determined by dividing the χ by the erodibility constant and the reference drainage area raised to the m:

$$\tau = \frac{\chi}{KA_0^m},\tag{6}$$

and the relative rock uplift history (U^*) is converted to dimensional units (e.g., mm/yr) through:

$$U = U^* \left(K A_0^m \right). \tag{7}$$

We perform the inversion by discretizing the long profile for equal intervals of χ (\sim 500) because it allows for easier comparisons between adjacent basins. A sensitivity test (Figure S1) indicates a broad low misfit zone when the long profiles are inverted using 5–20 increments, which on average correspond to a χ -interval of 1,150 to 300. Thus, since the adopted χ interval of 500 falls within this range, it can be considered reasonable.

We carefully select basins that meet the below-listed assumptions. Under the assumption that spatial variations in K are mostly related to changes in rock type, we only chose drainage basins with uniform or comparable rock types to maximize the likelihood that variations in $k_{\rm sn}$ are related to base level fall change rather than spatial changes in rock type. H, the small size of the analyzed basins (at most several tens of km²) suggests that spatial variations in rock uplift rate within each basin are minimized in this setting. We also assume that drainage networks are relatively static and do not suffer from substantial drainage area gain or loss. Under these assumptions, knickpoints are assumed to be transient, and the result of changes in base level fall rate (e.g., rock uplift rate) are identified as breaks in slope between two linear segments in χ -plots as well as spikes in inverted χ - $k_{\rm sn}$ and τ -U plots. Furthermore, these assumptions, along with maps of the long term (e.g., Plio-Pleistocene) rock uplift (U; e.g., Arisco et al., 2006), allow us to get rough approximations of K, assuming U and E are roughly balanced over the long term, using Equation 4 and basin average $k_{\rm sn}$. Uncertainties in $k_{\rm sn}$ and E were propagated into calculations of E and E using a bootstrap analysis sampled 1,000 times within a range of 20% around the average values.

4. Results

The geomorphic analysis enables quantitative characterization of landscape dynamics in Sicily (Figure S2) and allows us to detect those portions of the landscape experiencing geomorphic transients. The regional morphometric analysis (Figures 4, S4, and S5–S10) shows an E-W trending belt of high $k_{\rm sn}$, up to 27 m^{0.9}, for streams draining the Tyrrhenian (northern) flank of the PMNPM (Figure 4b). This high $k_{\rm sn}$ belt stands out from the low background values of 4 m^{0.9} characterizing the rest of the Island, in particular its westernmost edge and the whole southern side of Sicily, including part of the south-flowing drainages (Figure 3b). Other $k_{\rm sn}$ hotspots include the Piano Battaglia area (PB in Figure 4b), where limestones locally outcrop, and the area around S. Marco D'Alunzio (SMdA in Figures 4b and S8), where active faulting has been documented (Meschis et al., 2018; Pavano et al., 2012, 2015). To the east, moderate $k_{\rm sn}$ values of up to 15 m^{0.9}, characterize the channels draining the Ionian slope of the Peloritani Mts. (Figure 4b), whereas to the west, in the Palermo Mountains, $k_{\rm sn}$ is rather low (10 m^{0.9}). The patterns observed for northern Sicily in maps of other morphometrics, including topographic dissection (T_D) , local relief (L_R) , and hypsometric integral (HI), generally mimic the patterns of $k_{\rm sn}$ and are thus discussed in detail in the supplement for brevity (Figures S4 and S5-S10). To the south, along the entire central belt of Sicily, a geomorphic boundary, defined by a band of moderate $k_{\rm sn}$ values between 6 and 15 m^{0.9}, can be drawn from the Sicanian Mts. region in the west up to the southern flank of Mt. Etna to the east (Figure 4b).

Variations in \mathcal{X} values along divides are co-located with changes in $k_{\rm sn}$ and the relief indices ($L_{\rm R}$, $T_{\rm D}$, and HI; Figures 4b, 4c, S4, and S5–S10). High cross-divide \mathcal{X} contrasts (up to 9; Figure 4c) are noted across the PMNPM main divide, with higher values along channel heads that drain the southern flank. The high \mathcal{X} drainages roughly correspond with the area between the two main E–W-oriented lineaments detected in the $k_{\rm sn}$ map. Here, the main rivers are optimally oriented (E–W) to record the impact of the eastward translation of the Calabrian forearc (inset of Figure 4c, see dashed box for location). Although minor, contrasts in \mathcal{X} (up to 3; red lines in inset in Figure 4c) systematically occur on the northern flanks of the headwaters of the

PAVANO AND GALLEN 8 of 20



main WNW-ESE-trending tributaries of the Simeto and Gornalunga rivers, depicting a general southward valley asymmetry.

Rivers draining the Tyrrhenian (northern) flank of Sicily show two knickpoints (Figures 5f–5l). Knickpoints are demarcated in Figure 5 as abrupt increases in U (or $k_{\rm sn}$) as a function of τ (Figures 5a–5e) and changes in the slope of best-fit forward models of the inversion results in χ -elevation space (black line in Figure 5f–5l). Based on the inverse modeling of river profiles, these features emerge as two peaks in uplift rate (or $k_{\rm sn}$) and represent two distinct west-to-east time transgressive base level fall events (BLF_{old} and BLF_{young}). Although not directly quantifiable due to the bias imposed by the Tikhonov regularization used for the inversion, the uncertainties associated with the best-fit curve in the -elevation plots reflect the uncertainties in the reconstructed rock uplift signals. Since the best-fit profile is the integral of the uplift history, uncertainties on the predicted elevation increase with increasing age. Some of the knickpoints are more prominent than others, so we classify them as principal knickpoints; the more subtle, minor knickpoints are labeled mkp in Figure 5. The minor knickpoints are distinguished from the principal ones because of their less pronounced change in $k_{\rm sn}$ (Figures 5a–5e and S11). The sets of knickpoints are laterally correlated among the catchments on the basis of comparable χ -values ranges (i.e., 1,000–2,000; 2,000–4,000), but are at systematically higher χ and τ in the western drainages in the Palermo Mts. than in the eastern drainages of the Peloritani mountains (Figures 5a–5e and S11).

Several general inferences can be drawn from the analysis of these two knickpoint sets as a function of time and distance along the coastline moving from west-to-east (Figure 6c). First, the general magnitude of the rate of inferred base level fall generally increases for both knickpoint sets moving from west to east (circle size in Figure 6c). Second, the timing of both inferred base level fall events declines from west to east (Figure 6c). BLF_{old} (first pulse of rock uplift) is modeled to have started 4 Ma in the west and 1 Ma in the east, whereas BLF_{young} youngs eastward from 2 to 0.5 Ma (Figures 5a–5e, 6a–6c, and S11). Third, the time range between base level fall events systematically declines from west to east from 2 to 0.3 Myr (inset in Figure 6c). Finally, the rate at which the transient perturbations that generated each knickpoint set traveled along the northern coast of Sicily can be determined by the slope of a linear regression fit through τ -distance along the coast data (Figure 6c). This analysis suggests that the older perturbation represented by the upper, older knickpoints traveled at a rate of 4 cm/yr, and the younger perturbation traversed the coastline at a rate of 10 cm/yr (Figure 6c).

To better illustrate the west-to-east time transgressive patterns, we calculate the cumulative rock uplift from the river profile inversions in one million year increments from 4 to 1 Ma and plot the results as a function of basin outlet distance eastward of the reference point noted in Figure 6a. This way, the results are analogous to the pattern of cumulative rock uplift and deformation of marine terraces of 4 to 1 Ma. Further, we plot the rock uplift rate along this west-to-east transect in increments of 4–1 Ma (Figure 6b). Both plots illustrate a rock uplift signal increasingly located towards the east along Northern Sicily.

5. Discussion

The geomorphic analyses collectively indicate that the northern Sicily landscape is the most dynamic portion of the entire region; the drainage system and topography are characterized by larger and more prominent geomorphic transients than the rest of the Island. As in all landscapes, climate, rock-type, and tectonics collectively contribute to the observed geomorphic processes and topography. However, along northern Sicily, the alignment of transient fluvial knickpoints and the related distribution of topographic metrics are most consistent with a history of time-transgressive base level fall driven by spatially variable and temporally unsteady crustal deformation. Below we outline the assumptions in the river profile inversion and further describe justifications for why a specific assumption is met within the studied drainage basin. We then proceed with a detailed interpretation of the recovered signal in the context of the competing geodynamic models for Calabrian forward translation during the late Cenozoic. This is followed by a discussion of the geomorphic response to the interpreted tectonic forcing inferred from topographic proxies for drainage divide dynamics. We conclude with a discussion of the study implications for understanding the geodynamic evolution of this region since 4 Ma.

PAVANO AND GALLEN 9 of 20



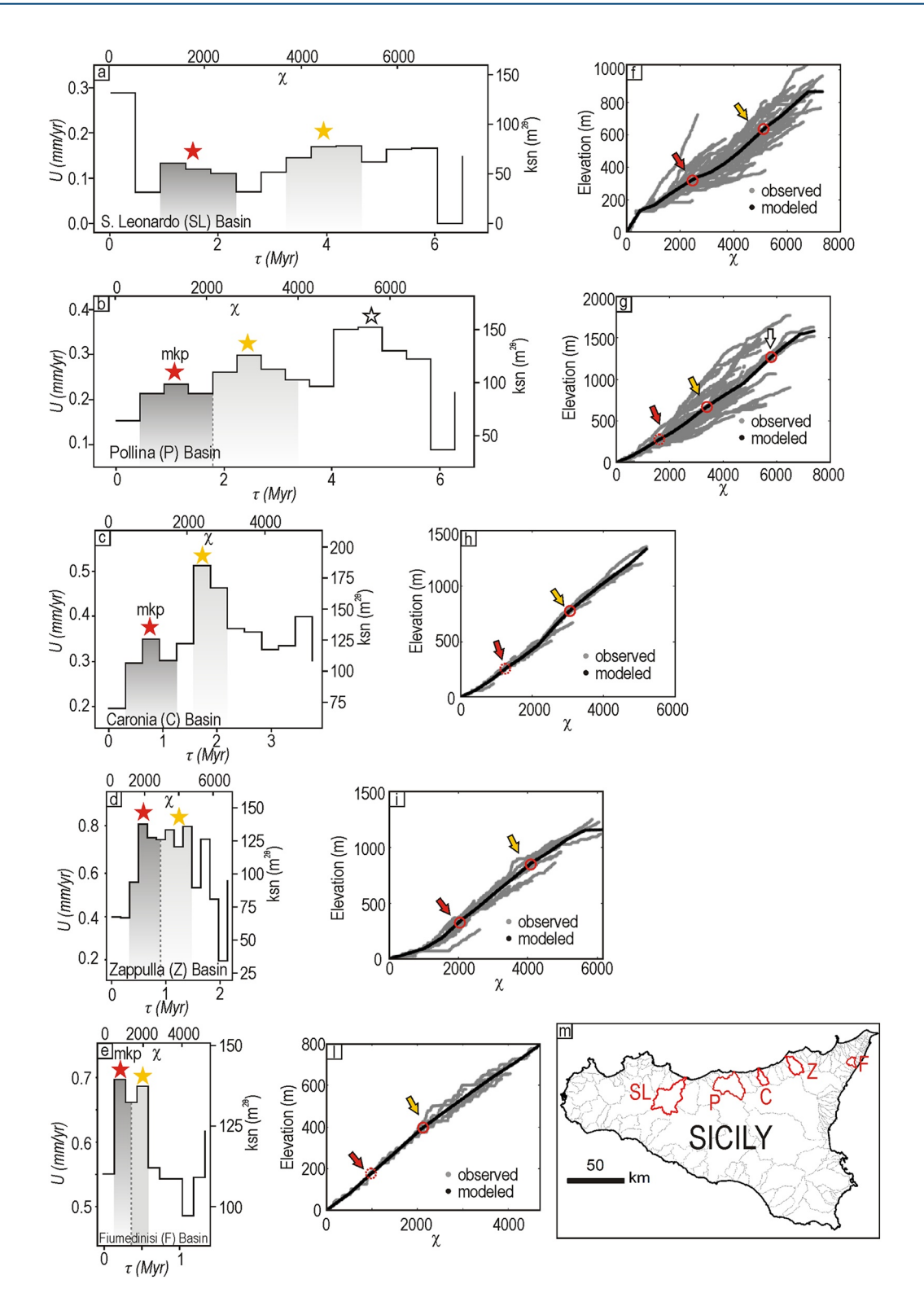


Figure 5

PAVANO AND GALLEN 10 of 20



5.1. River Profile Inversion Assumptions

In order to reliably interpret the river long profile inversions, we must ensure that some assumptions are reasonably justified. Here, we are mainly concerned with spatial variations in rock-type and rock uplift rate across the study region, but we also consider the potential impact of sea level variations and divide motion rate on interpretation of the results. In northern Sicily, precipitation and rock-type distributions show little evidence of large changes coincident with topographic metrics variations (e.g., Figure 1b). At least on the catchment scale, rock-type is relatively uniform, suggesting spatial changes in rock erodibility (K) are minimal. We note that studies have shown that K can co-vary with rock uplift on the regional scale, but here, even though this is the case (Figure S3), we assume these variations are negligible at the catchment scale (e.g., Pavano et al., 2016; Snyder et al., 2000). Along PMNPM, rock uplift rate changes spatially from west to east at a regional scale and through time. The spatial variations are assumed to be large relative to the small size of the drainages considered here. We thus make the simplifying assumption that the temporal history of rock uplift recorded in each basin can be approximated with a block uplift scheme. Given that the assumptions of spatially and temporally invariant K and spatially uniform U appear justified for each individual basin, we can interpret river profile geometry changes as primarily reflecting the history of base level fall (rock uplift) and use the block uplift inverse model of Goren et al. (2014) to recover the uplift history. The consistency of the rock uplift histories obtained for adjacent basins provides support that these assumptions are reasonable (Table 1).

The calibrated response time of the rivers is short enough (maximum typically of 4 Myr; Table 1) such that they do not record the drastic drawdown during the Messinian Salinity Crisis at ca. 5–6 Ma recorded in the offshore bathymetry (e.g., Micallef et al., 2019). In addition, we do not see evidence of relatively high-frequency base level fluctuations associated with mid-late Pleistocene glacio-eustatic sea level rise and fall in the river profiles (e.g., many small knickpoints moving through the drainage networks). This observation is perhaps not surprising given the modeling results of Snyder et al. (2002) that during the Quaternary, the rate of sea level rise and fall is typically too fast relative to the fluvial response time to generate a suite of upstream migrating knickpoints related to sea level oscillations. This finding was echoed by Gallen and Fernández-Blanco (2021), who showed that even under circumstances designed to amplify a sea level signal in river profile morphology, the impact of sea level change is secondary to longer-term changes in tectonically driven rock uplift rate. Furthermore, the time and space scale of observation and modeling resolution are not sensitive to <1 Ma glacio-eustatic base level changes (cf., Pavano et al., 2016). We, therefore, interpret the signals of base level fall recorded in the northern Sicily river networks as the result of geodynamically driven variations in rock uplift.

The inverse modeling of river profiles as conducted here assumes static drainage network configurations. However, there is evidence of active divide motion indicated by the cross-divide asymmetries in χ (Figure 4c), suggesting that this assumption is not correct. Nonetheless, the divide migration rates are probably slow as there is little evidence of large-scale river captures. Furthermore, it has been demonstrated that when the divide migration rate is slow, as appears to be the case in Sicily, relative to the fluvial response time, river profiles remain faithful recorders of tectonic activity (e.g., Whipple et al., 2017). However, we acknowledge that divide migration introduces an unconstrained amount of uncertainty in the analysis, which we infer is small relative to the tectonic signals recovered.

Figure 5. (a–e) River response time (τ) -rock uplift/ k_{sn} plots showing the results of five of the 11 long profile inversions performed for the northern Sicily's drainage basins, stacked according to a west-to-east distribution. The uncertainties associated to the rock uplift signals increase with age, as suggested by the increase in the uncertainties of the best-fit curve (black line) in (f–l). The χ values are reported in the x axis at the top, and the k_{sn} values in the y axis to the right. Red and yellow stars indicate knickpoints (mkp stands for minor knickpoint) paired with young and old base level fall events, respectively. The white star in the Pollina basin's plot indicates a third peak, not detected in the other profiles, suggesting either an earlier base level pulse or a local change in rock type; The red star in the Fiumedinisi basin's plot indicating the younger base level fall could be related to the activation of the Taormina normal fault bounding the Ionian coast of the Peloritani ridge; (f–l) χ -elevation plots showing the observed and the modeled (χ -transformed) long profile (black line). The colored arrows indicate the location of knickpoints associated with the corresponding peaks (colored stars) in the U- τ plots; the red circles indicate the location of the slope change in the modeled (sometimes smoothed) long profile (black line) associated to the knickpoints (dotted red circle for the mkp); (m) map showing the location of the drainage profiles of figure (a–e).

PAVANO AND GALLEN 11 of 20

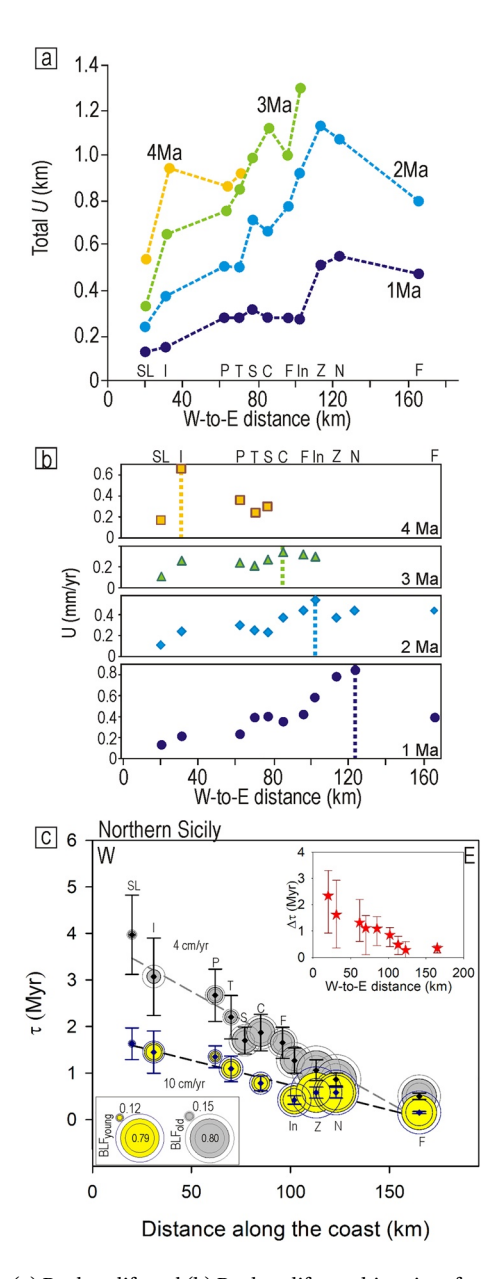


Figure 6. (a) Rock uplift and (b) Rock uplift rate histories of northern Sicily reconstructed by inverting the long profiles of the different analyzed basins, distributed west-to-east. The data are shown for subsequent 1Myr steps of the last 4 Myr evolution of the area. In (b), the dashed lines indicate the location where the maximum value of rock uplift has been modeled for the different landscape evolutionary stage; (c) west-to-east distribution of the response time (τ) values of the main peaks (BLF_{old}, gray circles, and $\ensuremath{\mathsf{BLF}_{\mathsf{young}}}\xspace$, yellow circles) recognized along the different inversion curves of the analyzed basins. The circles (black line) are sized according to the modeled rock uplift; the values in the inset in the left bottom corner of the figure are references for the minimum (small circle) and the maximum (large circle) rock uplift value. The circles are also buffered according to the estimated uncertainties (see Table S3). The inset at the top shows the west-to-east distribution of the time gap between any τ_{old} and τ_{young} couple. Basins: SL: San Leonardo, I: Imera, P: Pollina, T: Tusa, S: Santo Stefano, C: Caronia, F: Furiano, In: Inganno, Z: Zappulla, N: Naso, F: Fiumedinisi.

5.2. Rock Uplift Signal Interpretation

Along the northern belt of Sicily, the modeled, time-averaged long-term rock uplift rate changes from 0.15–0.45 mm/yr, in the west, to 0.4–0.9 mm/yr, in the east, varying temporally as well, over the Quaternary (Figure 6b). The data presented in Figures 6a and 6b illustrates a rock uplift signal progressively moving from west to east across northern Sicily. This generally smooth, progressively eastward migrating pattern is most consistent with the crustal wave hypothesis summarized by Model A (Figure 3e). We note that the general eastward increase in the magnitude of these signals likely reflects the slightly oblique trajectory of the Calabrian forearc approaching the African paleo-margin (Figures 2a and 2c). Minor variations in the along-coast uplift patterns probably reflect local deformation along minor upper-crustal faults. In particular, at 1 Ma, the sharp drop in uplift rate at the eastern end of the study area would coincide with the fault system at the transition between the Nebrodi and the Peloritani Mts. (Figure 6b; e.g., Cammarata et al., 2018; Pavano et al., 2015).

The tectonic imprint along northern Sicily is evident in the distribution of high channel steepness $(k_{\rm sn})$ values (Figure 4b), depicting a W-E-trending alignment of knickpoints along the PMNPM (Figure 4b), and of the other geomorphic metrics (e.g., L_R , HI, and channel slope; Figure S4). Overall, the values of these geomorphic metrics progressively increase toward the east (Figures S5-S10). Most importantly, the W-E pattern of the timing of knickpoint genesis (i.e., base level fall events) of the rivers draining the northern flank of the PMNPM shows a uniformly eastward decreasing trend (Figure 6c). This finding provides crucial support for Model A's predictions (Figures 2d, and 3e, and 3g). Interestingly, the observations diverge slightly from some predictions of Model A; the two observed knickpoints become systematically more closely spaced in time moving eastward rather than maintaining a consistent time difference as predicted by Model A (Figures 3g and 6). Furthermore, the magnitude of rock uplift appears to systematically increase eastward (circle's size in Figure 6c), matching coastal rock uplift patterns recovered by Pleistocene marine terraces (Antonioli et al., 2006; Catalano & De Guidi, 2003; Catalano & Di Stefano, 1997; Sulli et al., 2013).

In addition to the general distribution parallel to the main regional-scale tectonic boundaries (Catalano, Pavano, et al., 2018; Ghisetti & Vezzani, 1984; Figure 4b), locally, within the PMNPM, the geomorphic patterns highlight some discontinuities between adjacent sectors (Figures S4 and 4b). Although, these disruptions in the patterns are subtle, and they do not seem to have a regional-scale importance and sothward lateral continuity beyond the PMNPM (e.g., Figures S8–S10). Collectively the uplift pattern as recorded by river profiles draining the northern coast of Sicily is most consistent with the crustal wave model presented in Figures 3e and 3g.

5.3. Interpretation of the Geomorphic Response

The patterns observed in the χ analysis can be interpreted in the context of the inferred spatial and temporal rock uplift history (Figure 4c). The χ map suggests that the PMNPM's divide should be moving south, away from the coast, but such differences in χ could be driven by non-uniform uplift (Figure 4c; e.g., Forte & Whipple, 2018). However, application of

PAVANO AND GALLEN 12 of 20

Table 1Main Estimations of the Response Time (τ) and Rock Uplift Rate (U)
History Results Coming From the Inversion of the Long Profiles Performed for the Main Drainage Systems Draining Northern Sicily

Basins	τ _o (Myr)	U _o (mm/a)	τ _y (Myr)	U _y (mm/a)	τ_{o} - τ_{y} (Myr)	$K (m^{0.1} \text{ yr}^{-1})$
SanLeonardo	3.97	0.15	1.63	0.12	2.34	2.56E-06
Torto						2.46E-06
Imera	3.07	0.28	1.45	0.38	1.62	3.01E-06
Pollina	2.67	0.32	1.35	0.22	1.32	2.72E-06
Tusa	2.20	0.26	1.09	0.39	1.11	2.90E-06
Sstefano	1.70	0.51				3.32E-06
Caronia	1.87	0.56	0.78	0.36	1,09	3.12E-06
Furiano	1.65	0.48				3.10E-06
Inganno	1.27	0.56	0.42	0.56	0.85	4.00E-06
Zappulla	1.06	0.77	0.58	0.79	0.48	6.48E-06
Naso	0.86	0.81	0.58	0.79	0.28	7.06E-06
Fiumedinisi	0.5	0.69	0.15	0.70	0.35	6.91E-06

 $\it Note:$ $_{\rm o}$ and $_{\rm y}$ refers to $\rm BLF_{\rm old}$ and $\rm BLF_{\rm young}$ base level fall episodes accounted for the different curves.

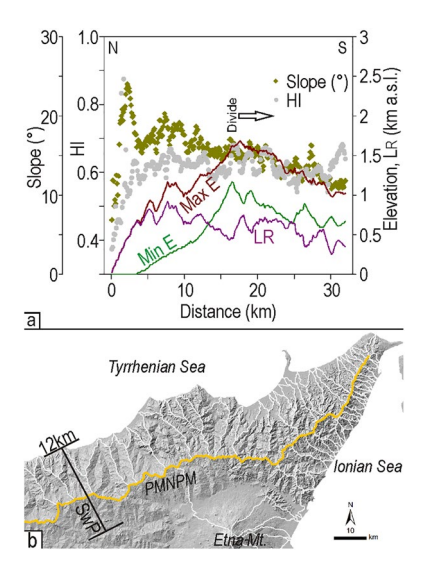


Figure 7. (a) Geomorphic metrics sampled by swath profile across the PMNPM (trace in Figure 7b). LR: Local Relief; Max E: maximum elevation; Min E: minimum elevation. The empty black arrow indicates the sense of the divide's migration as suggested by the χ -analysis; (b) map showing the location of the 12 km-wide swath profile (SwP) of Figure (a) and the regional drainage divide of eastern PMNPM (yellow line).

the Gilbert metrics, which are argued to be better metrics for divide mobility (Forte & Whipple, 2018; Whipple et al., 2017), with the addition of $k_{\rm sn}$, $T_{\rm D}$, and HI (Figures 7a, 7b, 4b, and S4), are consistent with divide motion directions inferred from χ . Based on this consistency, we interpret that the divide is migrating southward in response to base level fall at the coast.

That base level fall is time transgressive, moving from west to east (Figure 6c), and this dynamic history of uplift should affect PMNPM divide motion in space and time. Guided by results from a landscape evolution model experiment by Forte and Whipple (2018), a migrating wave of rock uplift, as inferred to have impacted northern Sicily, would result in an early northward migration of the divide, corresponding to northward enlargement of southern drainage basins. Once the tectonic perturbation passes, the rock uplift gradient across the PMNPM divide drops. The relaxation of the across-divide rock uplift gradient would then result in the southward migration of the main divide to regain equilibrium. A snapshot of this process is perhaps what is observed today along the PMNPM and depicted by the west-to-east distribution of the main relief metrics (Figures S6–S10).

The transit of the Calabrian forearc high would have also impacted the region south of the PMNPM, in eastern Sicily (inset in Figure 4c). Here, the cross-divide χ -contrasts characterizing the Gornalunga and Simeto basins suggest a southward migrating divide (Figure 4c), consistent with valley asymmetry due to crustal accretion, associated with the active eastward migration of the Calabrian forearc high. We highlight that the patterns of divide migration observed along the PMNPM divide and basins to the south are generally consistent with expectations of the wave of rock uplift predicted by Model A.

5.4. Tectonic Interpretations

There is a general consistency in the W–E patterns observed in the geomorphic analyses conducted here (Figures 4b, 5, 6, S4, and S5–S10) and both the Bouguer gravimetric anomalies and the Moho depth gradient in northern Sicily (Ferri et al., 2005; Giustiniani et al., 2018; Figure 1c). The similarity in spatial patterns supports the idea that the roughly W–E-oriented crustal structures (e.g., Kumeta-Alcantara Line; Ghisetti & Vezzani, 1984) played a role in accommodating the eastward migration of the Calabrian forearc high. Nevertheless, the PMNPM shows local variations (e.g., Figure 4b) in basin average geomorphic metrics that correspond with local distributions in the total rock uplift signal (Figure 6a). We associate these variations with minor, subsidiary Riedel shear faults conjugated along major W–E-trending regional-scale tectonic boundaries and partially accommodating crustal fragmentation and extension, as corroborated by earthquake focal mechanisms confined in the northern belt of Sicily (Billi et al., 2010; Cammarata et al., 2018; Scarff et al., 2016).

Within the context of the crustal wave model (Model A, Figure 3), the two tectonic rock uplift pulses (BLF $_{\rm old}$ and BLF $_{\rm young}$), affecting northern Sicily during the last 4 Myr (Figures 5a–5e, 6c, and S11; Table 1) can be interpreted as a result of coupled, diachronous crustal and asthenospheric responses associated with the eastward-migrating Calabrian forearc. The older pulse of uplift is interpreted as a result of crustal accretion and thickening on the leading edge of the migrating forearc that is followed

PAVANO AND GALLEN 13 of 20



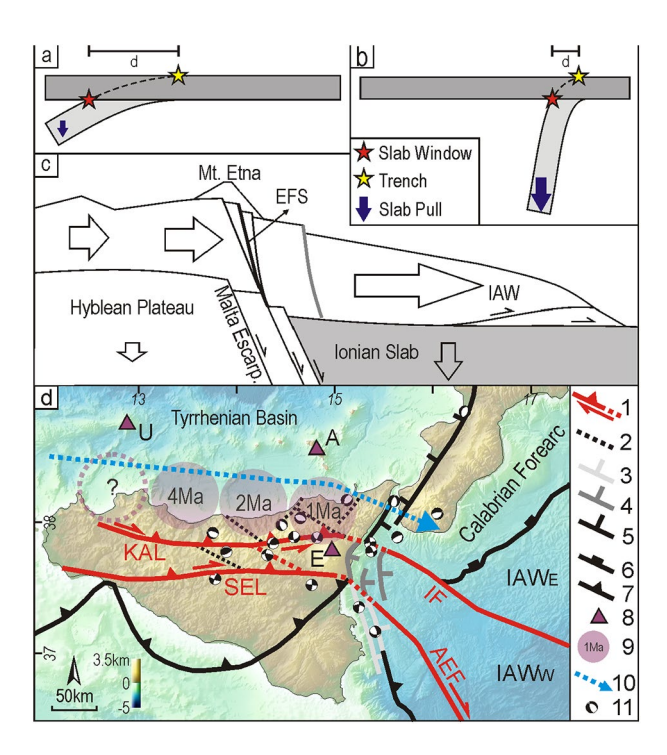


Figure 8. Schematic model of both trench and slab window/tearing retreat focusing on their relative distance (d) according to (a) low and (b) high slab pull; (c) schematic NW-SE-oriented section across Mt. Etna, showing the kinematic threshold corresponding to the extensional belt of the Etna Fault System (EFS) that accommodates the faster migration of the Ionian Accretionary Wedge (IAW); (d) schematic geodynamic model compatible with the presented geomorphic data. 1: Strike-slip fault (dashed where hypothesized); triangles indicate the vertical component of movement; 2: minor crustal fault; 3: Reactivated Malta Escarpment; 4: normal faults serving as a kinematic threshold accommodating the eastward escape of the Sicilian accretionary wedge; 5: extensional belt of the Calabrian forearc high; 6: Calabrian forearc; 7: Front of the allochthonous units; 8: Volcanic centers (A: Aeolian Archipelago; (e) Etna Volcano; U: Ustica); 9: estimated position (and modeled age) of the tectonic pulses (dashed outline where hypothesized) linked to the Plio-Pleistocene transit of the Calabrian forearc; 10: approximate trajectory of the southern termination of the Calabrian arc; 11: Focal mechanisms (modified from Barreca et al., 2016; Loreto et al., 2012; Musumeci et al., 2005; Pondrelli et al., 2006; Scarfí et al., 2016). KAL: Kumeta-Alcantara Line (Ghisetti & Vezzani, 1984); SEL: Sicanian-Etna Line (Catalano, Pavano, et al., 2018); IF: Ionian Fault (Polonia et al., 2016); AEF: Alfeo-Etna Fault (Gallais et al., 2013; Polonia et al., 2012); IAW: Ionian Accretionary Wedge, E: eastern lobe, W: western lobe.

by a temporary decline in rock uplift rate associated with subsequent normal faulting. The second, young pulse of uplift is thought to be related to the eastward tearing of the Ionian slab and subsequent asthenospheric inflow through a slab window at the rear of the Calabrian forearc (e.g., Faccenna et al., 2005, 2007, 2011; Palano et al., 2017; Wortel et al., 2009; Figure 6c). We note that the 1.5–2 Ma transit of the more recent rock uplift pulse (BLF $_{young}$) at the western Madonie Mts. (Figure 6c) is consistent with the occurrence of early Pliocene deposits found by Abate et al. (1991) at an elevation of about 1.6 km a.s.l. This observation suggests a long-term rock uplift rate of about 0.3–0.45 mm/yr, consistent with the river profile inversion results presented here (Table S3).

Based on the discussion above, we view the geomorphic observations in northern Sicily as analogous to the crustal conveyor models proposed for the migration of the Mendocino Triple Junction (MTJ) in the western USA (e.g., Furlong & Govers, 1999). In the MTJ, a northward migrating wave of rock uplift is thought to be related to ephemeral crustal thickening-thinning cycles due to the passage of the MTJ. Here, we infer that the first base level fall signal is associated with crustal thickening as the forearc approaches a given point along the coastline. Uplift rates then slowly decline as the crustal wave passes. The second pulse of uplift is interpreted to be associated with asthenospheric convection at depth (e.g., Neumann et al., 2015) that occurs as the hydrated, low-viscosity mantle wedge encroaches beneath a given point along the coast.

The river profile inversions allow us to determine migration rates of the two modeled waves of rock uplift, traveled eastward at nearly steady rates of 4 and 10 cm/yr (Figure 6c), matching the available independent estimates for the Calabrian trench's rollback (Malinverno & Ryan, 1986; Rosenbaum & Lister, 2004) and the main spreading rates of the Tyrrhenian Basin (i.e., Vavilov and Marsili volcanic stages; Figures 2b and 2c; Guillaume et al., 2010; Marani & Trua, 2002; Nicolosi et al., 2006). With the support of previous work, we speculate on the cause of the progressively decreasing time range between the two rock uplift pulses (inset in Figure 6c). We can link this decreasing time gap to the acceleration of the eastward propagating slab tearing and narrowing processes (Faccenna et al., 2005, 2007; Scarff et al., 2018; Wortel et al., 2000), likely due to the increase in the slab pull force during the progressive slab collapse in the asthenosphere (Figures 8a and 8b; Faccenna et al., 2004, 2011; Schellart, 2004; Wortel et al., 2009).

5.5. Final Remarks on the Geodynamic Model

The geomorphic setting depicted in the present work, framed in the context of the west-to-east migration of the Calabrian forearc, allows spec-

ulation on the relationships between the main shear zones of the region, as well as a revision of their importance and role in controlling three main sectors of eastern Sicily. To the north, the stretching of the NE-Sicily corner is directly affected by the upper plate dynamics connected to the transit of the Calabrian forearc high and consequent mantle dynamics at depth. The area immediately to the south (inset in Figure 4c) corresponds to the accreting and eastward-migrating (Figure 1d) wedge of central-eastern Sicily, interpreted as a thickened crustal domain roughly confined between two major dextral shear zones: the Kumeta-Alcantara Line (Ghisetti & Vezzani, 1984), to the north, and the Sicanian-Etna Line (Catalano, Pavano, et al., 2018), to the south (Figures 4b and 8d). The extension affecting the eastern edge of this region can be envisioned as resulting from a spatially fixed kinematic threshold accommodating the wedge squeezed between the forearc and the buoyant Hyblean crustal spur and finally free to move faster to the

PAVANO AND GALLEN 14 of 20



southeast onto the subducting Ionian slab (Figure 8c). Such dynamics would be accommodated by known NW–SE-oriented dextral strike-slip faults and roughly N–S-trending normal faults (Bousquet et al., 1988; Catalano et al., 2004, 2017; Hirn et al., 1991; Monaco et al., 1997, 2005; Tortorici et al., 2013, 2021) currently affecting the eastern flank of Mt. Etna. Here, these relatively shallow kinematics would overlap the lithospheric WNW–ESE-trending crustal stretching of the Ionian near offshore of SE-Sicily (Catalano et al., 2008; Monaco & Tortorici, 2000), which accommodate the differential slab-pull between the Ionian slab and the buoyant Hyblean lithosphere (lithospheric tear fault; Figure 8d). Overall, these inferences would suggest that the inland prolongation of the faults detected in the Ionian offshore (e.g., Ionian Fault; IF in Figure 8d) could be sought along major E–W-oriented shear zones.

6. Conclusion

Two tectonic rock uplift cycles, occurring in the last 4 Ma, are inferred from long profile inversion analysis performed for the main drainage basins of northern Sicily. The results indicate west-to-east time transgressive polycyclic tectonic pulses that are inferred to have occurred in response to crustal thickening-thinning cycles due to mantle dynamics following the transit of the Calabrian forearc. Asthenospheric convection reorganization in the upper plate mantle wedge and subduction slab tearing dynamics appear a likely cause of later stage isostatic rebound and subsequent crustal fragmentation. The geomorphic transience recorded in the topography of northern Sicily is well depicted by relatively high $k_{\rm sn}$ values, distributed along belts parallel to the mountain belt of northern Sicily, and by the strong cross-divide χ -contrast related to the southward roaming of the regional divide, as corroborated by the distribution of other relief metrics (e.g., L_R , T_D , and HI). Discrete changes in landscape morphology and topographic metrics are not observed. This suggests that the main NW-SE-oriented shear zones, and the minor NE-SW-trending faults, would represent polycyclic Neogene-Quaternary crustal lineaments conjugated to major W-E-oriented tectonic boundaries. The resulting kinematic model emphasizes these latter as leading, at a lithospheric scale, the eastward migration of the Calabrian forearc's system. Thus, the structural architecture reconstructed by previous studies for the adjacent Ionian Basin's area should be extended inland along these W-E-trending major structures. Importantly, the geomorphic approach used in the present work might serve as a model that can be more broadly applied to explore collisional and subduction zone boundaries in other geodynamic settings around the globe.

Data Availability Statement

The digital elevation model data that support the findings of this study are available through ISPRA (www.sinanet.isprambiente.it). The Matlab codes that support this research are archived in the Zenodo repository publisher, https://doi.org/10.5281/zenodo.431796510.5281/zenodo.4317965, and are available through GitHub at https://github.com/sfgallen/Block_Uplift_Linear_Inversion_Models. Additional plots, figures, and small tables are published with the manuscript as supporting information.

Acknowledgments

The authors would like to thank Editor Taylor Schildgen, Associate Editor Duna Roda-Boluda, and Luca Malatesta and an anonymous reviewer for their helpful and constructive comments that improved the earlier version of this manuscript. The authors also would like to thank Frank J. Pazzaglia for the productive discussions about data and for the comments and the informal revision of an early version of the manuscript. We also thank Benjamin Bliss, James Fisher, and Ethan Kurak. This paper has been promoted by the support from the National Science Foundation, under the grant 1904262 (TESPRESSO Project, PI: F.J. Pazzaglia).

References

Abate, B., Di Stefano, E., Incandela, A., & Renda, P. (1991). Evidenze di una fase tettonica pliocenica nelle Madonie occidentali (Sicilia centro-settentrionale). *Memorie della Societa Geologica Italiana*, 47, 225–234.

Amodio Morelli, L., Bonardi, G., Colonna, V., Dietrich, D., Giunta, G., Ippolito, F., et al. (1976). L'arco calabro-peloritano nell'orogene appenninico-maghrebide. *Memorie della Societa Geologica Italiana*, 17, 1–60.

Antonioli, F., Kershaw, S., Renda, P., Rust, D., Belluomini, G., Cerasoli, M., et al. (2006). Elevation of the last interglacial highstand in Sicily (Italy): A benchmark of coastal tectonics. *Quaternary International*, 145–146, 3–18.

Argnani, A., & Bonazzi, C. (2005). Malta Escarpment fault zone offshore eastern Sicily: Pliocene-Quaternary tectonic evolution basedon new multichannel seismic data. *Tectonics*, 24, TC4009. https://doi.org/10.1029/2004TC001656

Barreca, G., Scarfi, L., Cannavò, F., Koulakov, I., & Monaco, C. (2016). New structural and seismological evidence and interpretation of a lithospheric-scale shear zone at the southern edge of the Ionian subduction system (central-eastern Sicily, Italy). *Tectonics*, 35(6), 1489–1505.

Barreca, G., Scarfi, L., Gross, F., Monaco, C., & De Guidi, G. (2019). Fault pattern and seismotectonic potential at the south-western edge of the Ionian Subduction system (southern Italy): New field and geophysical constraints. *Tectonophysics*, 761, 31–45.

Ben Avraham, Z., Boccaletti, M., Cello, G., Grasso, M., Lentini, F., Torelli, L., & Tortorici, L. (1990). Principali domini strutturali originatesi dallacollisione neogenico-quaternaria nel Mediterraneo centrale. Memorie della Societa Geologica Italiana, 45, 453–462.

PAVANO AND GALLEN 15 of 20



- Bianchi, F., Carbone, S., Grasso, M., Invemizzi, G., Lentini, F., Longareni, G., et al. (1987). Sicilia orientale: Profilo geologico Nebrodi-Iblei. Memorie della Società Geologica Italiana, 38, 429–458.
- Bigi, G., Bonardi, G., Catalano, R., Cosentino, D., Lentini, F., Parotto, M., et al. (1991). Structural model of Italy scale 1:500.000, sheet 6. C.N.R., Progetto Finalizzato Geodinamica. SELCA Firenze.
- Billi, A., Presti, D., Orecchio, B., Faccenna, C., & Neri, G. (2010). Incipient extension along the active convergent margin of Nubia in Sicily, Italy: Cefal-Etna seismic zone. *Tectonics*, 29(4), TC4026.
- Boccaletti, M., Cello, G., & Tortorici, L. (1990). Strike-slip deformation as a fundamental process during the Neogene-Quaternary evolution of the Tunisian-Pelagian area. *Annales Tectonicae*, 4, 104–119.
- Bonforte, A., Catalano, S., Maniscalco, R., Pavano, F., Romagnoli, G., Sturiale, G., & Tortorici, G. (2015). Geological and geodetic constraints on the active deformation along the northern margin of 826 the Hyblean Plateau (SE Sicily). *Tectonophysics*, 640, 80–89. http://dx.doi.org/10.1016/j.tecto.2014.11.024
- Bousquet, J. C., Lanzafame, G., & Pasquin, C. (1988). Tectonic stress and volcanism: In situ stress measurements and neotectonics investigations in the Etna area (Italy). *Tectonophysics*, 149, 219–231.
- Burollet, P. F., Mugniot, G. M., & Sweeney, P. (1978). Geology of the Pelagian Block: The margin and basin of Southen Tunisia and Tripolitania. In A. Nairn, W. Kanes, & F. G. Stelhi (Eds.), *The ocean basin and margin* (pp. 331–419). Plenum.
- Cammarata, L., Catalano, S., Gambino, S., Palano, M., Pavano, F., Romagnoli, G., et al. (2018). Seismological and structural constraints on the 2011–2013, Mmax 4.6 seismic sequence at the south-eastern edge of the Calabrian arc (North-eastern Sicily, Italy). *Geomorphology*, 723. 56–67.
- Carminati, E., & Doglioni, C. (2012). Alps vs. Apennines: The paradigm of a tectonically asymmetric Earth. *Earth-Science Reviews*, 112, 67–96.
- Catalano, R., & D'Argenio, B. (1982). Guida alia geologia della Sicilia occidentale. Società Geologica Italiana, Guide Geologiche Regionali, 9–41.
- Catalano, R., Franchino, A., Merlini, S., & Sulli, A. (2000). Central western Sicily structural setting interpreted from seismic reflection profiles. *Memorie della Societá Geologica Italiana*, 55, 5–16.
- Catalano, R., Valenti, V., Albanese, C., Accaino, F., Sulli, A., Tinivella, U., et al. (2013). Sicily's fold-thrust belt and slab rollback: The SI.RI. PRO. seismic crustal transect. *Journal of the Geological Society*, 170, 451–464. https://doi.org/10.1144/jgs2012-099
- Catalano, S., Cirrincione, R., Mazzoleni, P., Pavano, F., Pezzino, A., Romagnoli, G., & Tortorici, G. (2018). The effects of a Meso-Alpine collision event on the tectono-metamorphic evolution of the Peloritani mountain belt (eastern Sicily, southern Italy). Geological Magazine, 155(2), 422–437.
- Catalano, S., & De Guidi, G. (2003). Late Quaternary uplift of northeastern Sicily: Relation with the active normal faulting deformation. Journal of Geodynamics, 36, 445–467. https://doi.org/10.1016/S0264-3707(02)00035-2
- Catalano, S., De Guidi, G., Monaco, C., Tortorici, G., & Tortorici, L. (2008). Active faulting and seismicity along the Siculo-Calabrian rift zone. *Tectonophysics*, 453, 177–192. https://doi.org/10.1016/j.tecto.2007.05008
- Catalano, S., Pavano, F., Romagnoli, G., & Tortorici, G. (2017). Late Quaternary tectonics and active ground deformation in the Catania urban area (eastern Sicily): New constraints from a geological investigation. *Tectonophysics*, 712–713, 200–207.
- Catalano, S., Pavano, F., Romagnoli, G., Tortorici, G., & Tortorici, L. (2018). Late Tortonian-Quaternary tectonic evolution of central Sicily: The major role of the strike-slip deformation. *Geological Magazine*, 155(2), 536–548.
- Catalano, S., Torrisi, S., & Ferlito, C. (2004). The relationship between Late Quaternary deformation and volcanism of Mt. Etna (eastern Sicily): New evidence from the sedimentary substratum in the Catania region. *Journal of Volcanology and Geothermal Research*, 132, 311–344.
- Chironi, C., De Luca, L., Guerra, I., Luzio, D., Moretti, A., Vitale, M., & Group SEALAND. (2000). Crustal structures of the Southern Tyrrhenian Sea and the Sicily Channel on the basis of the M25, M26, M28, M39WARR profiles. *Bollettino della Società Geologica Italiana*. 119. 189–203.
- Conti, A., Bigi, S., Cuffaro, M., Doglioni, C., Scrocca, D., Muccini, F., et al. (2017). Transfer Zone in an oblique back-arc basin setting: Insights from the Latium-Campania segmented margin (Tyrrhenian Sea). *Tectonics*, 36, 78–107. https://doi.org/10.1002/2016TC004198
- D'Agostino, N., D'Anastasio, E., Gersavi, A., Guerra, I., Nedimović, M. R., Seeber, L., & Steckler, M. S. (2011). Forearc extension and slow rollback of the Calabrian Arc from GPS measurements. *Geophysical Research Letters*, 38, L17304. https://doi.org/10.1029/2011GL048270
- Decima, A., & Wezel, F. C. (1971). Osservazioni sulle evaporiti messiniane della Sicilia centro-meridionale. Rivista Mineraria Siciliana, 130–132, 172–187
- Dewey, J. F., Helman, M. L., Turco, E., Hutton, D. H. W., & Knott, S. D. (1989). Kinematics of the western Mediterranean. In M. P. Coward, D. Dietrich, & R. G. Park (Eds.), *Alpine tectonics* (pp. 265–283). Geological Society of London, Special Publication.
- Di Grande, A., & Giandinoto, V. (2002). Plio-Pleistocene sedimentary facies and their evolution in centre-southeastern Sicily: A working hypothesis. EGU Stephan Mueller Special Publication Series, 1, 211–221.
- Doglioni, C. (1993). Geological evidence for a global tectonic polarity. Journal of the Geological Society, 150, 991–1002.
- Elter, P., Giglia, G., Tongiorgi, M., & Trevisan, L. (1975). Tensional and compressional areas in the recent (Tortonian to present) evolution of the Northern Apennines. *Bollettino di Geofisica Teorica ed Applicata*, 17, 3–18.
- Faccenna, C., Becker, T. W., Auer, L., Billi, A., Boschi, L., Brun, J. P., et al. (2014). Mantle dynamics in the Mediterranean. Reviews of Geophysics, 52, 283–332.
- Faccenna, C., Civetta, L., D'Antonio, M., Funiciello, F., Margheriti, L., & Piromallo, C. (2005). Constraints on mantle circulation around the deforming Calabrian slab. *Geophysical Research Letters*, 32, L06311. https://doi.org/10.1029/2004GL021874
- Faccenna, C., Funiciello, F., Civetta, L., D'Antonio, M., Moroni, M., & Piromallo, C. (2007). Slab disruption, mantle circulation, and the opening of the Tyrrhenian basins. In L. Beccaluva, G. Bianchini, & M. Wilson (Eds.), Cenozoic volcanism in the Mediterranean area: Geological Society of America special paper 418 (pp. 153–169). https://doi.org/10.1130/2007.2418(08
- Faccenna, C., Molin, P., Orecchio, B., Olivetti, V., Bellier, O., Funiciello, F., et al. (2011). Topography of the Calabria subduction zone (southern Italy): Clues for the origin of Mt. Etna. *Tectonics*, 30, TC1003.
- Faccenna, C., Piromallo, C., Crespo-Blanc, A., Jolivet, L., & Rossetti, F. (2004). Lateral slab deformation and the origin of the western Mediterranean arcs. *Tectonics*, 23, TC1012. https://doi.org/10.1029/2002TC001488
- Ferri, F., Ventura, R., Coren, F., & Zanolla, C. (2005). Note illustrative della Carta gravimetrica d'Italia in scala (Vol. 1, p. 14).
- Finetti, I. R. (2005). Deep seismic exploration of the Central Mediterranean and Italy CROP PROJECT (1st ed., Vol. 1, p. 794). Elsevier Science.
- Finetti, I. R., Lentini, F., Carbone, S., Catalano, S., & Del Ben, A. (1996). Il Sistema APPENNINO Meridionale-Arco Calabro-Sicilia Nel Mediterraneo centrale: Studio geologico-geofisico. Bollettino della Società Geologica Italiana, 115, 529–559.

PAVANO AND GALLEN 16 of 20



- Flint, J. J. (1974). Stream gradient as a function of order, magnitude, and discharge. Water Resources Research, 10, 969–973. https://doi.org/10.1029/WR010i005p00969
- Forte, A. M., & Whipple, K. X. (2018). Criteria and tools for determining drainage divide stability. *Earth and Planetary Science Letters*, 493, 102–117.
- Forte, A. M., & Whipple, K. X. (2019). Short communication: Short communication: The Topographic Analysis Kit (TAK) for TopoToolbox. Earth Surface Dynamics, 7, 87–95. https://doi.org/10.5194/esurf-7-87-2019
- Fox, M., Goren, L., May, D. A., & Willett, S. D. (2014). Inversion of fluvial channels for paleorock uplift rates in Taiwan. *Journal of Geophysical Research: Earth Surface*, 119(9), 1853–1875.
- Furlong, K. P., & Govers, R. (1999). Ephemeral crustal thickening at a triple junction: The Mendocino crustal conveyor. *Geology*, 27(2), 127–130.
- Gallais, F., Graindorge, D., Gutscher, M.-A., & Klaeschen, D. (2013). Propagation of a lithospheric tear fault (STEP) through the western boundary of the Calabrian accretionary wedge offshore eastern Sicily (southern Italy). *Tectonophysics*, 602, 141–152. https://doi.org/10.1016/j.tecto.2012.12.026
- Gallen, S. F., & Fernández-Blanco, D. (2021). A New Data-driven Bayesian Inversion of Fluvial Topography Clarifies the Tectonic History of the Corinth Rift and Reveals a Channel Steepness Threshold. *Journal of Geophysical Research: Earth Surface*, e2020JF005651. https://doi.org/10.1029/2020JF005651
- Gallen, S. F., & Thigpen, J. R. (2018). Lithologic controls on focused erosion and intraplate earthquakes in the eastern Tennessee seismic zone. *Geophysical Research Letters*, 45(18), 9569–9578.
- Ghisetti, F. C., & Vezzani, L. (1984). Thin-skinned deformations of the Western Sicily thrust belt and relationships with crustal shortening: Mesostructural data on the Mt. Kumeta Alcantara. *Bollettino della Società Geologica Italiana*, 103, 129–157.
- Giachetta, E., & Willett, S. (2018). A global dataset of river network geometry. Scientific Data, 5, 180127. https://doi.org/10.1038/sdata.2018.127
- Giustiniani, M., Tinivella, U., & Nicolich, R. (2018). Crustal structure of central Sicily. Tectonophysics, 722, 299-313.
- Gueguen, E., Tavarnelli, E., Renda, P., & Tramutoli, M. (2002). The geodynamics of the southern Tyrrhenian Sea margin as revealed by integrated geological, geophysical and geodetic data. *Bollettino della Società Geologica Italiana*, 1(1), 77–85.
- Guillaume, B., Funiciello, F., Faccenna, C., Martinod, J., & Olivetti, V. (2010). Spreading pulses of the Tyrrhenian Sea during the narrowing of the Calabrian slab. *Geology*, 38, 819–822. https://doi.org/10.1130/G31038.1
- Gutscher, M.-A., Dellong, D., Dominguez, S., Malavielle, J., Graindorge, D., & Klingelhoefer, F. (2019). Chapter 13 Strike-slip faulting in the Calabrian accretionary wedge: Using analog modeling to test the kinematic boundary conditions of geodynamic models. In J. C. Duarte (Ed.), *Transform plate boundaries and fracture zones* (pp. 321–337).
- Gutscher, M.-A., Dominguez, S., Mercier de Lepinay, B., Pinheiro, L., Babonneau, N., Cattaneo, A., et al. (2015). Tectonic expression of an active slab-tear from high-resolution seismic and bathymetric data offshore Sicily (Ionian Sea). *Tectonics*, 34, 39–54. https://doi.org/10.1002/2015TC003898
- Hack, J. T. (1957). Studies of longitudinal stream profiles in Virginia and Maryland (pp. 45–97). U.S. Geological Survey Professional Paper 294-B
- Hancock, G. S., Anderson, R. S., & Whipple, K. X. (1998). Beyond power: Bedrock river incision process and form. In K. J. Tinkler, & E. E. Wohl (Eds.), Rivers over rock: Fluvial processes in bedrock channels: American geophysical union geophysical Monograph 107 (pp. 35–60). https://doi.org/10.1029/GM107p0035
- Hirn, A., Nercessian, A., Sapin, M., Ferrucci, F., & Wittlinger, G. (1991). Seismic heterogenety of Mt. Etna structure and activity. *Geophysical Journal International*, 105, 139–153.
- Howard, A. D., & Kerby, G. (1983). Channel changes in badlands. Geological Society of America Bulletin, 94, 739–752. https://doi.org/10.1130/0016-7606(1983)94<739:CCIB>2.0
- ISPRA. (2004). IFFI database. Retrieved from http://www.isprambiente.govit/it/progetti/suolo-e-territorio-1/iffi-inventario-dei-fenomeni-franosi-in-italia Kastens, K. A., Mascle, J., Auroux, C., Bonatti, E., Broglia, C., Channell, J. E. T., et al. (1988). ODP Leg 107 in the Tyrrhenian Sea: Insights into passive margin and backarc basin evolution. Geological Society of America Bulletin, 100, 1140–1156.
- Kirby, E., & Whipple, K. X. (2001). Quantifying differential rock-uplift rates via stream profile analysis. *Geology*, 29, 415–418. https://doi.org/10.1130/0091-7613(2001)029<0415:QDRURV>2.0
- Lentini, F., & Carbone, S. (2014). Carta Geologica della Sicilia. 1:250.000. Memorie descrittive della Carta Geologica d'Italia, v. 95. Servizio Geologico d'Italia ISPRA.
- Lentini, F., Carbone, S., & Catalano, S. (1994). Main structural domains of the central Mediterranean region and their Neogene tectonic evolution. *Bollettino di Geofisica Teorica ed Applicata*, 36(141–144), 103–125.
- Lentini, F., Carbone, S., Catalano, S., & Grasso, M. (1995). Principali lineamenti strutturali della Sicilia nord-orientale. *Studi Geologici Camerti*, 2, 319–329.
- Lentini, F., Carbone, S., Catalano, S., & Grasso, M. (1996). Elementi per la ricostruzione del quadro strutturale della Sicilia orientale. *Memorie della Società Geologica Italiana*, 51, 179–195.
- Lentini, F., Catalano, S., & Carbone, S. (2000). Carta Geologica della Provincia di Messina. SELCA Firenze.
- Lentini, F., & Vezzani, L. (1975). Le unità meso-cenozoiche della copertura sedimentaria del basamento cristallino peloritano (Sicilia nord-orientale). Bollettino della Società Geologica Italiana, 94, 537-554.
- Loreto, M. F., Zgur, F., Facchin, L., Fracassi, U., Pettenati, F., Tomini, I., et al. (2012). In search of newimaging for historical earthquakes:

 A new geophysical survey offshore western Calabria (southern Tyrrhenian Sea, Italy). *Bollettino di Geofisica Teorica ed Applicata*, 53, 385–401.
- Malinverno, A. (2012). Evolution of the Tyrrhenian Sea-Calabrian Arc system: The past and the present. Rendiconti Online della Società Geologica Italiana, 21, 11–15.
- Malinverno, A., Cafiero, M., Ryan, W. B. F., & Cita, M. B. (1981). Distribution of Messinian sediments and erosional surfaces beneath the Tyrrhenian Sea: Geodynamic implications. *Oceanologica Acta*, 4, 489–495.
- Malinverno, A., & Ryan, W. B. F. (1986). Extension in the Tyrrhenian Sea and shortening in the Apennines as a result of arc migration driven by sinking of the lithosphere. *Tectonics*, 5, 227–245.
- Marani, M., & Trua, T. (2002). Thermal constriction and slab tearing at the origin of a super-inflated spreading ridge, Marsili volcano (Tyrrhenian Sea). *Journal of Geophysical Research*, 107, EPM 3-1-EPM 3-15. https://doi.org/10.1029/2001JB000285
- Mastrolembo Ventura, B., Serpelloni, E., Argnani, A., Bonforte, A., Bürgmann, R., Anzidei, M., et al. (2014). Fast geodetic strain-rates in eastern Sicily (southern Italy): New insights into block tectonics and seismic potential in the area of the great 1693 earthquake. Earth and Planetary Science Letters, 404, 77–88. https://doi.org/10.1016/j.epsl.2014.07.025

PAVANO AND GALLEN 17 of 20



- Meschis, M., Roberts, G. P., Mildon, Z. K., Robertson, J., Michetti, A. M., & Faure Walker, J. P. (2019). Slip on a mapped normal fault for the 28th December 1908 Messina earthquake (Mw 7.1) in Italy. Scientific Reports, 9(1), 6481. https://doi.org/10.1038/s41598-019-42915-2
- Meschis, M., Roberts, G. P., Robertson, J., & Briant, R. M. (2018). The relationships between regional Quaternary uplift, deformation across active normal faults, and historical seismicity in the upper plate of subduction zones: The Capo D'Orlando Fault, NE Sicily. *Tectonics*, 37, 1231–1255. https://doi.org/10.1029/2017TC004705
- Micallef, A., Camerlenghi, A., Georgiopoulou, A., Garcia-Castellanos, D., Gutscher, M. A., Lo Iacono, C., et al. (2019). Geomorphic evolution of the Malta Escarpment and implications for the Messinian evaporative drawdown in the eastern Mediterranean Sea. *Geomorphology*, 327, 264–283.
- Monaco, C., Catalano, S., De Guidi, G., & Tortorici, L. (2005). Geology of the urban area of Catania (Eastern Sicily). Advances in Earthquake Engineering Series, 14, 83–102.
- Monaco, C., & Tortorici, L. (2000). Active faulting in the Calabrian arc and eastern Sicily. Journal of Geodynamics, 29, 407-424.
- Montgomery, D. R., & Foufoula-Georgiou, E. (1993). Channel Network Source Representation Using Digital Elevation Models. Water Resource Research, 29, 3925–3934. https://doi.org/10.1029/93WR02463
- Musumeci, C., Patanè, D., Scarfi, L., & Gresta, S. (2005). Stress directions and shear-wave anisotropy: Observations from local earthquakes in southeastern Sicily Italy. *Bulletin of the Seismological Society of America*, 95(4), 1359–1374.
- Neumann, F., Vásquez-Serrano, A., Tolson, G., Negrete-Aranda, R., & Contreras, J. (2015). Toroidal, Counter-Toroidal, and Upwelling Flow in the Mantle Wedge of the Rivera and Cocos Plates: Implications for IOB Geochemistry in the Trans-Mexican Volcanic Belt. *Pure and Applied Geophysics*, 173, 3395–3417.
- Nicolich, R., Laigle, M., Hirn, A., Cernobori, L., & Gallart, J. (2000). Crustal structure of the Ionianmargin of Sicily: Etna volcano in the frame of regional evolution. *Tectonophysics*, 329, 121–139.
- Nicolosi, J., Speranza, F., & Chiappini, M. (2006). Ultrafast oceanic spreading of the Marsili Basin, southern Tyrrhenian Sea: Evidence from magnetic anomaly analysis. *Geology*, 34, 717–720. https://doi.org/10.1130/G22555.1
- Nigro, F., Renda, P., & Arisco, G. (2000). Tettonica recente nella Sicilia nord-occidentale e nelle Isole Egadi. *Bollettino della Società Geologica Italiana*, 119, 307–319.
- Osservatorio delle Acque. (2005). Regione Siciliana Assessorato Regionale dell'Energia e dei servizi di Pubblica Utilità. Retrieved from http://www.osservatorioacque.it
- Palano, M., Piromallo, C., & Chiarabba, C. (2017). Surface imprint of toroidal flow at retreating slab edges: The first geodetic evidence in the Calabrian subduction system. *Geophysical Research Letters*, 44, 845–853. https://doi.org/10.1002/2016GL071452
- Pavano, F., Catalano, S., Romagnoli, G., & Tortorici, G. (2012). Dynamics and seismotectonics of NE Sicily. Rendiconti Online della Società Geologica Italiana, 21, 241–243.
- Pavano, F., Pazzaglia, F. J., & Catalano, S. (2016). Knickpoints as geomorphic markers of active tectonics: A case study from northeastern Sicily (southern Italy). Lithosphere-US, 8(6), 633–648. https://doi.org/10.1130/L577.1
- Pavano, F., Romagnoli, G., Tortorici, G., & Catalano, S. (2015). Active tectonics along the Nebrodi-Peloritani boundary in northeastern Sicily (southern Italy). *Tectonophysics*, 659, 11. https://doi.org/10.1016/j.tecto.2015.07.024
- Pavano, F., Romagnoli, G., Tortorici, G., & Catalano, S. (2019). Morphometric evidences of recent tectonic deformation along the southeast-ern margin of the Hyblean Plateau (SE-Sicily, Italy). *Geomorphology*, 342, 1–19.
- Perron, J. T., & Royden, L. H. (2013). An integral approach to bedrock river profile analysis. *Earth Surface Processes and Landforms*, 38, 570–576. https://doi.org/10.1002/esp.3302
- Polonia, A., Torelli, L., Artoni, A., Carlini, M., Faccenna, C., Ferranti, L., et al. (2016). The Ionian and Alfeo-Etna fault zones: New segments of an evolving plate boundary in the central Mediterranean Sea? *Tectonophysics*, 675, 69–90. https://doi.org/10.1016/j.tecto.2016.03.016
- Polonia, A., Torelli, L., Gasperini, L., & Mussoni, P. (2012). Active faults and historical earthquakes in the Messina Straits area (Ionian Sea). Natural Hazards and Earth System Sciences, 12, 2311–2328. https://doi.org/10.5194/nhess-12-2311-2012
- Polonia, A., Torelli, L., Mussoni, P., Gasperini, L., Artoni, A., & Klaeschen, D. (2011). The Calabrian arc subduction complex in the Ionian Sea: Regional architecture, active deformation and seismic hazard. *Tectonics*, 30, TC5018. https://doi.org/10.1029/2010TC002821
- Pondrelli, S., Salimbeni, S., Ekström, G., Morelli, A., Gasperini, P., & Vannucci, G. (2006). The Italian CMT dataset from 1977 to the present. Physics of the Earth and Planetary Interiors. 159, 286–303.
- Pritchard, D., Roberts, G. G., White, N. J., & Richardson, C. N. (2009). Uplift histories from river profiles. *Geophysical Research Letters*, 36(24), L24301. https://doi.org/10.1029/2009GL040928
- Renda, P., Tavarnelli, E., Tramutoli, M., & Gueguen, E. (2000). Neogene deformations of northern Sicily, and their implications for the geodynamics of the Southern Tyrrhenian Sea margin. *Memorie della Societa Geologica Italiana*, 55, 53–59.
- Roberts, G. G., & White, N. (2010). Estimating uplift rate histories from river profiles using African examples. *Journal of Geophysical Research*, 115, B02406. https://doi.org/10.1029/2009JB006692
- Romagnoli, G., Catalano, S., Pavano, F., & Tortorici, G. (2015). Geological map of the Tellaro River Valley (Hyblean Foreland, southeastern Sicily, Italy). *Journal of Maps*, 66–74. https://doi.org/10.1080/17445647.2014.944878
- Rosenbaum, G., & Lister, G. S. (2004). Neogene and Quaternary rollback evolution of the Tyrrhenian Sea, the Apennines, and the Sicilian Maghrebides. *Tectonics*, 23, TC1013. https://doi.org/10.1029/2003TC001518
- Rosenbloom, N. A., & Anderson, R. S. (1994). Hillslope and channel evolution in a marine terraced landscape, Santa Cruz, California. Journal of Geophysical Research: Solid Earth, 99(B7), 14013–14029.
- Roure, F., Howel, D. G., Muller, C., & Moretti, I. (1990). Late Cenozoic subduction complex of Sicily. *Journal of Structural Geology*, 12, 250-266
- Sartori, R. (2003). The Tyrrhenian backarc basin and subduction of the Ionian lithosphere. Episodes, 26, 217-221.
- Sartori, R., Carrara, G., Torelli, L., & Zitellini, N. (2001). Neogene evolution of the southwestern Tyrrhenian Sea (Sardinia Basin and western Bathyal plain). *Marine Geology*, 175, 47–66. https://doi.org/10.1016/S0025-3227(01)00116-5
- Scarfi, L., Barberi, G., Barreca, G., Cannavó, F., Koulakov, I., & Patané, D. (2018). Slab narrowing in the Central Mediterranean: The Calabro-Ionian subduction zone as imaged by high resolution seismic tomography. Scientific Report, 8, 5178. https://doi.org/10.1038/s41598-018-23543-8
- Scarfi, L., Barberi, G., Musumeci, C., & Patané, D. (2016). Seismotectonics of northeastern Sicily and southern Calabria (Italy): New constraints on the tectonic structures featuring in a crucial sector for the central Mediterranean geodynamics. *Tectonics*, 35, 812–832. https://doi.org/10.1002/2015TC004022
- Schellart, W. P. (2004). Quantifying the net slab pull force as a driving mechanism for plate tectonics. *Geophysical Research Letters*, 31, L07611. https://doi.org/10.1029/2004GL019528

PAVANO AND GALLEN 18 of 20



Schwanghart, W., & Scherler, D. (2014). Short Communication: TopoToolbox 2 - MATLAB-based software for topographic analysis and modelling in Earth surface sciences. Earth Surface Dynamics, 2, 1–7. https://doi.org/10.5194/esurf-2-1-2014

10.1029/2020TC006692

- Schwanghart, W., & Scherler, D. (2017). Bumps in river profiles: Uncertainty assessment and smoothing using quantile regression techniques. Earth Surface Dynamics, 5, 821–839. https://doi.org/10.5194/esurf-5-821-2017
- Sgroi, T., De Nardis, R., & Lavecchia, G. (2012). Crustal structure and seismotectonics of central Sicily (southern Italy): New constraints from instrumental seismicity. *Geophysical Journal International*, 189, 1237–1252.
- Snyder, N. P., Whipple, K. X., Tucker, G. E., & Merritts, D. J. (2000). Landscape response to tectonic forcing: Digital elevation model analysis of stream profiles in the Mendocino triple junction region, northern California. *Geological Society of America Bulletin*, 112, 1250–1263. https://doi.org/10.1130/0016-7606(2000)112<1250:LRTTFD>2.0
- Snyder, N. P., Whipple, K. X., Tucker, G. E., & Merritts, D. J. (2002). Interactions between onshore bedrock-channel incision and nearshore wave-base erosion forced by eustasy and tectonics. *Basin Research*, 14(2), 105–127.
- Sulli, A., Lo Presti, V., Morticelli, M. G., & Antonioli, F. (2013). Vertical movements in NE Sicily and its offshore: Outcome of tectonic uplift during the last 125 ky. *Quaternary International*, 288, 168–182. https://doi.org/10.1016/j.quaint.2012.01.021
- Tortorici, G., Catalano, S., Pavano, F., & Romagnoli, G. (2013). History of the extensional deformation of the eastern flank of Mt. Etna: New insights from a detail field mapping. Rendiconti Online della Societá Geologica Italiana, 29, 179–182.
- Tortorici, G., Pavano, F., Romagnoli, G., & Catalano, S. (2021). The effect of recent resurfacing in volcanic areas on the distribution of co-seismic ground deformation due to strike-slip earthquakes: New insights from the 12/26/2018 seismic event at Mt. Etna. *Journal of Structural Geology*, 145, 104308.
- Tortorici, L., Monaco, C., Tansi, C., & Cocina, O. (1995). Recent and active tectonics in the Calabrian Arc (southern Italy). *Tectonophysics*, 243, 37–55.
- Whipple, K. X. (2004). Bedrock rivers and the geomorphology of active orogens. *Annual Review of Earth and Planetary Sciences*, 32, 151–185, https://doi.org/10.1146/annurey.earth.32.101802.120356
- Whipple, K. X., Forte, A. M., DiBiase, R. A., Gasparini, N. M., & Ouimet, W. B. (2017). Timescales of landscape response to divide migration and drainage capture: Implications for the role of divide mobility in landscape evolution. *Journal of Geophysical Research: Earth Surface*, 122, 248–273.
- Whipple, K. X., Hancock, G. S., & Anderson, R. S. (2000). River incision into bedrock: Mechanics and relative efficacy of plucking, abrasion, and cavitation. *Geological Society of America Bulletin*, 112, 490–503. https://doi.org/10.1130/0016-7606(2000)112<490:R IIBMA>2.0.CO;2
- Whipple, K. X., & Tucker, G. E. (1999). Dynamics of the stream power river incision model: Implications for height limits of mountain ranges, landscape response timescales and research needs. *Journal of Geophysical Research*, 104(17), 661–717. https://doi.org/10.1029/1999JB900120
- Willett, S. D., McCoy, S. W., Perron, J. T., Goren, L., & Chen, C.-Y. (2014). Dynamic reorganization of river basins. *Science*, 343, 1248765. https://doi.org/10.1126/science.1248765
- Wobus, C., Whipple, X. K., Kirby, E., Snyder, N., Johnson, J., Spyropolou, K., et al. (2006). Tectonics from topography: Procedures, promise, and pitfalls. In S. D. Willett, N. Hovius, M. T. Brandon, & D. M. Fisher (Eds.), Tectonics, climate, and landscape evolution: Geologica Society of America special paper 398, Penrose Conference series, pp. 55–74. https://doi.org/10.1130/2006.2398(04)
- Wortel, M. J. R., Govers, R., & Spakman, W. (2000). Subduction and slab detachment in the Mediterranean- 1320 Carpathian region. Science. 290. 1910–1917.
- Wortel, M. J. R., Govers, R., & Spakman, W. (2009). Continental collision and the STEP-wise evolution of convergent plate boundaries: From structure to dynamics. In S. Lallemand & F. Funicello (Eds.), Subduction zone geodynamics (pp. 47–59). Springer.

References From the Supporting Information

- Ardizzone, F., Basile, G., Cardinali, M., Casagli, N., Del Conte, S., Del Ventisette, C., et al. (2012). Landslide inventory map for the Briga and the Giampilieri catchments, NE Sicily, Italy. *Journal of Map*, 8(2), 176–180.
- Arisco, G., Arnone, G., Favara, R., Nigro, F., Perricone, M., Renda, P., & Mondello, C. (2006). Integrated neotectonic and morphometric analysis of northern Sicily. *Bollettino della Società Geologica Italiana*, 125(2), 221–244.
- Bianca, M., Monaco, C., Tortorici, L., & Cernobori, L. (1999). Quaternary normal faulting in southeastern Sicily (Italy): A seismic source for the 1693 large earthquake. *Geophysical Journal International*, 139, 370–394.
- Bull, W. B. (1991). Geomorphic responses to climatic change (p. 326). Oxford University Press.
- Catalano, S., & Di Stefano, A. (1997). Sollevamento e tettogenesi Pleistocenica lungo il margine tirrenico dei Monti Peloritani: Integrazione dei dati geomorfologici, strutturali e biostratigrafici. *Il Quaternario Italian Journal of Quaternary Sciences*, 10, 337–342.
- Catalano, S., Romagnoli, G., & Tortorici, G. (2010). Kinematics and dynamics of the Late Quaternary rift-flank deformation in the Hyblean Plateau (SE Sicily). *Tectonophysics*, 486, 1–14. https://doi.org/10.1016/j.tecto.2010.01.013
- Catalano, S., Torrisi, S., Tortorici, G., & Romagnoli, G. (2011). Active folding along a rift-flank: The Catania region case history (SE Sicily). Journal of Geodynamics, 51, 53–63.
- Drummond, R. H., & Dennis, H. W. (1968). Qualifying relief terms. The Professional Geographer, 20(5), 326-332.
- Faccenna, C., Piromallo, C., Crespo-Blanc, A., Jolivet, L., & Rossetti, F. (2004). Lateral slab deformation and the origin of the Western Mediterranean arcs. *Tectonics*, 23, TC1012. https://doi.org/10.1029/2002TC001488
- Ferranti, L., Antonioli, F., Anzidei, M., Monaco, C., & Stocchi, P. (2010). The timescale and spatial extent of vertical tectonic motions in Italy: Insights from relative sealevel changes studies. In M. Beltrando, A. Peccerillo, M. Mattei, S. Conticelli, & C. Doglioni (Eds.), *The geology of Italy. Journal of the virtual explorer* (Vol. 36, p. 1441). Electronic Edition Paper 30.
- Gallen, S. F. (2018). Lithologic controls on landscape dynamics and aquatic species evolution in post-orogenic mountains. Earth and Planetary Science Letters, 493, 150–160. https://doi.org/10.1016/j.epsl.2018.04.029
- Goren, L., Fox, M., & Willett, S. D. (2014). Tectonics from fluvial topography using formal linear inversion: Theory and applications to the Inyo Mountains, California. *Journal of Geophysical Research: Earth Surface*, 119(8), 1651–1681. https://doi.org/10.1002/2014JF003079
- Lifton, N. A., & Chase, C. G. (1992). Tectonic, climatic, and lithologic influences on landscape fractal dimension and hypsometry—Implications for landscape evolution in the San Gabriel Mountains, California. *Geomorphology*, 5, 77–114. https://doi.org/10.1016/0169-555X(92)90059-W
- Monaco, C., Tapponnier, P., Tortorici, L., & Gillot, P. Y. (1997). Late Quaternary slip rates on the Acireale-Piedimonte normal faults and tectonic origin of Mt. Etna (Sicily). Earth and Planetary Science Letters, 147, 125–139.

PAVANO AND GALLEN 19 of 20



- Pavano, F. (2013). Late Quaternary deformation of NE Sicily from relief and drainage system analysis. *Rendiconti Online della Società Geologica Italiana*, 29, 134–137.
- Pavano, F., Catalano, S., Romagnoli, G., & Tortorici, G. (2018). Hypsometry and relief analysis of the southern termination of the Calabrian arc, NE-Sicily (southern Italy). *Geomorphology*, 304, 74–88.
- Pike, R. J., & Wilson, S. E. (1971). Elevation-relief ratio, hypsometric integral and geomorphic area-altitude analysis, *The Geological Society of America Bulletin*. (Vol. 82, pp. 1079–1084). https://doi.org/10.1130/0016-7606(1971)82[1079:ERHIAG]2.0.CO;2
- Schilirò, L., Esposito, C., & Scarascia Mugnozza, G. (2015). Evaluation of shallow landslide-triggering scenarios through a physically based approach: An example of application in the southern Messina area (northeastern Sicily, Italy). *Natural Hazards and Earth System Sciences*, 15, 2091–2109.
- Strahler, A. N. (1952). Hypsometric (area-altitude) analysis of erosional topology. The Geological Society of America Bulletin, 63(11), 1117–1142.
- Walcott, R. C., & Summerfield, M. A. (2008). Scale dependence of hypsometric integrals: An analysis of southeast African basins. *Geomorphology*, 96, 174–186.
- Willgoose, G., & Hancock, G. (1998). Revisiting the hypsometric curve as an indicator of form and process in transport-limited catchment. Earth Surface Processes and Landforms, 23, 611–623.

PAVANO AND GALLEN 20 of 20